International Journal of Biological Macromolecules 321 (2025) 146114

Contents lists available at ScienceDirect

International Journal of Biological Macromolecules

journal homepage: www.elsevier.com/locate/ijbiomac

Structural characterization and biotechnological potential of an exopolysaccharide produced by *Bacillus licheniformis* F2LB isolated from Fumarole Bay of Deception Island, Antarctica

Aparna Banerjee [a,*,1], João Paulo Fabi [b,c,1], Catherine Ormeño [a], Srijan Banerjee [d], Nicolás Flores-Castañón [e], Francisca Valenzuela [e], Shrabana Sarkar [a], Alexander Galán [f,g], Dipayan Samanta [h], Priya Saxena [h], Rajesh K. Sani [h], Manik Prabhu Narsing Rao [i], Gustavo Cabrera-Barjas [j]

[a] Functional Polysaccharides Research Group, Instituto de Ciencias Aplicadas, Facultad de Ingeniería, Universidad Autónoma de Chile, Sede Talca, Talca, Chile
[b] Department of Food Science and Experimental Nutrition, School of Pharmaceutical Sciences, University of São Paulo, São Paulo, SP, Brazil
[c] Food Research Center (FoRC), CePID-FAPESP (Research, Innovation and Dissemination Centers, São Paulo Research Foundation), CEPIX, São Paulo, SP, Brazil
[d] PhD Program in Science, R&D Bioactive Products Department, Chemistry Institute of Natural Resources, University of Talca, Talca, Chile
[e] Doctorado en Ciencias Biomédicas, Instituto de Ciencias Biomédicas, Facultad de Ciencias de la Salud, Universidad Autónoma de Chile, Talca, Chile
[f] Centro de Investigación de Estudios Avanzados del Maule (CIEAM), Vicerrectoría de Investigación y Postgrado, Universidad Católica del Maule, Talca, Chile
[g] Centro Regional de Estudios Ambientales (CREA), Universidad Católica de la Santísima Concepción, Concepción, Chile
[h] Karen M. Swindler Department of Chemical and Biological Engineering, South Dakota School of Mines and Technology, Rapid City, SD 57701, USA
[i] Instituto de Ciencias Aplicadas, Facultad de Ingeniería, Universidad Autónoma de Chile, Sede Talca, Talca 3460000, Chile
[j] Facultad de Ciencias de la Rehabilitación y Calidad de Vida, Universidad San Sebastián, Campus Las Tres Pascualas, Lientur 1457, 4080871 Concepción, Chile

ARTICLE INFO

Keywords:
Bacillus licheniformis
Antarctic exopolysaccharide
Structural characterization
Antioxidant activity
Emulsifying properties
Food biotechnology

ABSTRACT

Deception Island, Antarctica, harbors unique polyextreme conditions fostering versatile microorganisms with significant biotechnological potential. This is due to genomic adaptation to extreme conditions that lead to metabolic alterations, such as the production of unique exopolysaccharides. *Bacillus licheniformis* F2LB, isolated from Deception Island, Antarctica, was evaluated for its exopolysaccharide's structural and biotechnological potential (EPS). Genome analysis revealed EPS biosynthesis, UV resistance, and thermal adaptation genes. The EPS with a putative glucogalactomannan backbone, comprised mainly of a sugar molar ratio Man: Glu: Xyl: Fuc (1: 0.7: 0.4: 0.3) and other sugars in trace amounts. Spectroscopy identified key glycosidic linkages, and morphology showed a rough, nonporous surface. Functionally, EPS demonstrated robust thermal stability (T_{peak} 255 °C), remarkable antioxidant activities (~100 % H_2O_2 scavenging; DPPH: 75.5 %), good emulsifying ability (90 % in olive oil), and water (238.7 %) and oil-holding capacities (384.7 %) exceeding commercial xanthan gum. These findings underline its potential as a sustainable food additive.

1. Introduction

Polyextreme ecosystems are physiologically and biologically different from single extreme environments due to the co-existence of more than one extreme condition, which influences gene expression in various ways. This forces microorganisms to survive under multiple stresses at once. Microorganisms develop special metabolic and physiological abilities to cope with these harsh conditions, allowing them to thrive and produce bioactive compounds with several significant contributions in recent biotechnological advancements [1–4]. Among these compounds, exopolysaccharides (EPSs) are particularly notable for their antioxidant, anti-inflammatory, immunostimulant, and emulsifying properties. Their stability at high temperatures, extreme pH, and salinity makes them ideal for industrial applications [1,5–7]. For instance, the food industry seeks value-added compounds from natural sources that can offer enhanced functionality and bioactivity, promoting healthier options for consumers [5,8,9]. The natural food additives market has seen significant growth since the last century, realizing the

* Corresponding author.
E-mail address: aparna.banerjee@uautonoma.cl (A. Banerjee).
[1] Both the authors contributed equally to the paper.

https://doi.org/10.1016/j.ijbiomac.2025.146114
Received 13 December 2024; Received in revised form 14 July 2025; Accepted 16 July 2025
Available online 17 July 2025

recognized benefits of biologically active compounds and raising concerns over the risks of artificial additives [10]. Bacterial EPSs are complex polysaccharides composed of branched and repeating sequences of sugars like galactose, mannose, fructose, glucose, rhamnose, etc., and their derivatives are included in different proportions, which are produced massively outside of the bacterial cell wall in stressful environments. In harsh environments, EPS shields microbial cells from dehydration, osmotic stress, toxic substances, and phage attacks and plays a crucial role in facilitating communication between cells [11].

The *Bacillus* genus consists of a wide range of endospore-forming, rod-shaped, Gram-positive bacteria with significant applied biology applications in pharmaceutical, agriculture, and the food industry [12]. Thermophilic *Bacillus* species like *B. alcalophilus*, *B. amyloliquefaciens*, *B. clausii*, *B. cereus*, *B. brevis*, *B. halodurans*, *B. lentus*, *B. licheniformis*, *B. subtilis*, *and B. stearothermophilus*, are commonly abundant in high-temperature ecosystems. These severe habitats include craters of volcanoes, geothermal regions, hot springs, mining sites, hot mud, composting areas, and locations of deep-sea hydrothermal vents. Mostly, they live in temperatures ranging from 60 to 80 °C [13]. According to a previously published report, *B. licheniformis* EPS BL-P2 showed good radical scavenging activity and inhibited α-glucosidase and α-amylase enzymes [14]. To improve the shelf life of processed food, EPSs are perceived as good natural antioxidants that can also stabilize oil-water emulsions. Recently, the *B. licheniformis* MS3 strain was reported to have >60 % emulsification index in cottonseed oil [15]. EPS isolated from *B. albus* DM-15 strain was reported previously to have >60 % emulsification in xylene [16].

Our study emphasizes the structural characterization and analysis of the biotechnological potential of a novel exopolysaccharide produced by *Bacillus licheniformis* F2LB isolated from Fumarole Bay of Deception Island in Antarctica, which shows good potential to be used as a food additive in the future. Antarctica features poly-extreme environmental conditions such as the co-existence of extreme UV radiation, temperature variances, extreme salinity, and snow coverage conditions [17,18]. Despite Antarctica's predominantly cold environment, it also contains active volcanoes that host diverse microorganisms. Currently, there are two active volcanoes in Antarctica (https://www.livescience.com/planet-earth/volcanos/antarctica-is-covered-in-volcanoes-could-they-erupt, accessed on 8-12-2024). One active volcano is in Maritime Antarctica (Deception Island) [19–21]. Deception Island, a marine back-arc stratovolcano located in the South Shetland Islands within the Bransfield Basin [22,23], stands out as a unique part of Antarctica due to its distinctive environmental conditions, which include both icy and hot habitats [21,24,25]. This island differs from continental volcanoes due to its marine influence and higher temperatures, with areas near fumaroles reaching up to 100 °C [21,26]. This volcanic island hosts polar volcanoes that foster the creation of fumaroles, which exhibit extreme temperature gradients over very short distances, reaching temperatures up to 100 °C and subzero temperatures adjacent to the glaciers [21,24,25]. Fumarole Bay is one of the largest fumarole fields in Deception Island, with geothermal anomalies having temperatures ranging from 90 to 110 °C with rich emissions of hydrogen sulfide and carbon dioxide [24]. In addition, abundant geothermal activity makes Deception Island a fascinating equivalent of an extraterrestrial environment [23,27]. The island's uniqueness makes it a hotspot for understanding microbes and their unique bioactive compounds in extreme conditions. Various studies have been carried out to understand the microbial diversity of Deception Island [23,25,28]. In addition, Antarctic Deception Island has also been studied for different thermophilic microbial enzymes, namely nitrilase [29], superoxide dismutase [30], and lipases [31]. However, the bacterial EPS isolated from Antarctica, specifically from Deception Island, has been less explored. Keeping this in context, in the present study, we focused on exploring the uniqueness of the microbiota of Deception Island, EPS production by the thermophilic bacteria, its characterization, and technological application.

The primary aim of this study was to structurally characterize and explore the biotechnological potential of a novel exopolysaccharide (EPS) produced by *Bacillus licheniformis* F2LB isolated from the poly-extreme environment of Fumarole Bay, Deception Island, Antarctica. The novelty lies in identifying unique structural features and functional properties of this EPS, attributed to genomic adaptations of extremophilic microorganisms to severe environmental conditions such as extreme temperatures and UV radiation. This research is important as it reveals new bioactive compounds with significant potential for industrial applications, particularly as sustainable food additives exhibiting antioxidant and emulsifying properties.

2. Materials and methods

2.1. Study site, sample collection and in-situ analysis

Samples were obtained from the interstitial water (at 30 cm depth approx.) of the thermal anomalies found in the coastal marine intertidal zone of Fumarole Bay (62°58′6.1″S; 60°42′32.7″W), located in the west of Deception Island in northern Antarctica (Fig. 1). The sample was collected in austral summer (26th December 2022) as part of Chilean Antarctic Expedition (ECA 59) with the logistic support of Spanish Gabriel de Castilla (GdC) base. It is important to note that in order to facilitate access to the thermal anomalies, the sampling was carried out during low tide. In situ physiochemical parameters such as temperature, salinity, conductivity, pH, total dissolve solids and redox potential were measured using a multiparametric probe (BLE-pH 01, Shenzhen Yago, China), while UV radiometer (UV340B, Shenzhen Sanpo Instrument, China) was used to measure the UV (UVA + UVB) radiation. Water samples for analysis of nitrate (NO_3^-), nitrite (NO_2^-), silicate (SiO_4^{4-}) and orthophosphate (PO_4^{3-}), were filtered through 0.7 μm nominal pore size glass-fiber filters (GFF) and frozen at −20 °C until analysis. NO_3^-, PO_4^{3-}, and SiO_4^{4-} were analyzed following Atlas et al. [32], while NO_2^- was determined via spectrophotometry following Strickland and Parsons [33,34]. Samples were run in triplicate in an autoanalyzer manufactured in the Pontificia Universidad Católica de Valparaíso, Chile. The relative standard error for NO_3^-, NO_2^-, PO_4^{3-}, and SiO_4^{4-} was lower than ±10, ±3, ±3, and ± 5 %, respectively. Greenhouse gases – GHG (CO_2, CH_4, and N_2O) were measured in triplicate from water collected in 20 mL crimp-cap glass vials, using saturated $HgCl_2$ to fix the samples. Samples were stored at dark and room temperature until analysis. GHG were determined by gas chromatography using the headspace technique [35] in a gas chromatograph (Greenhouse GC-2014, Shimadzu) equipped with a methanizer to convert CO_2, a flame ionization detector (FID) for CH_4 and an electron capture detector (ECD) for N_2O. The coefficient of variation of the GHG measurements was <3 %.

2.2. Isolation and polyphasic characterization of the EPS producing thermophilic bacteria

To isolate thermophilic bacteria, a serial dilution was performed, with 50 μL from each dilution aseptically inoculated into Luria Bertani (LB) broth and incubated at 55 °C. After 24 h of incubation, a white, opaque, circular colony with undulate and mucoid characteristics was selected for further experiments. The salt tolerance of the isolate was tested across a range of NaCl concentrations from 0 to 8 %. The optimal pH for growth was assessed by adjusting the medium's pH between 5 and 9 using 1 M HCl and 1 M NaCl [36], followed by incubation at 55 °C. Cell growth was monitored spectrophotometrically at 590 nm. Additionally, the antibiotic sensitivity of the fumarolic isolate was evaluated using the disc diffusion method against 4 kits of broad-spectrum antibiotics from HiMedia, India which are Hexa G-minus 11 containing Amikacin (AK) 30 μg, Ampicillin (AMP) 10 μg, Ampicillin/Sulbactum (A/S) 10/10 μg, Ceftriaxone (CTR) 30 μg, Ofloxacin (OF) 5 μg, and Ticarcillin/Clavulanic Acid (TCC); Hexa G-minus 2 containing Ceftazidime (CAZ) 30 μg, Ciprofloxacin (CIP) 5 μg, Amikacin (AK) 30 μg, Nitrofurantoin (NIT) 300 μg, Netillin (NET) 30 μg, and Nalidixic acid (NA) 30 μg; Hexa G-plus 2

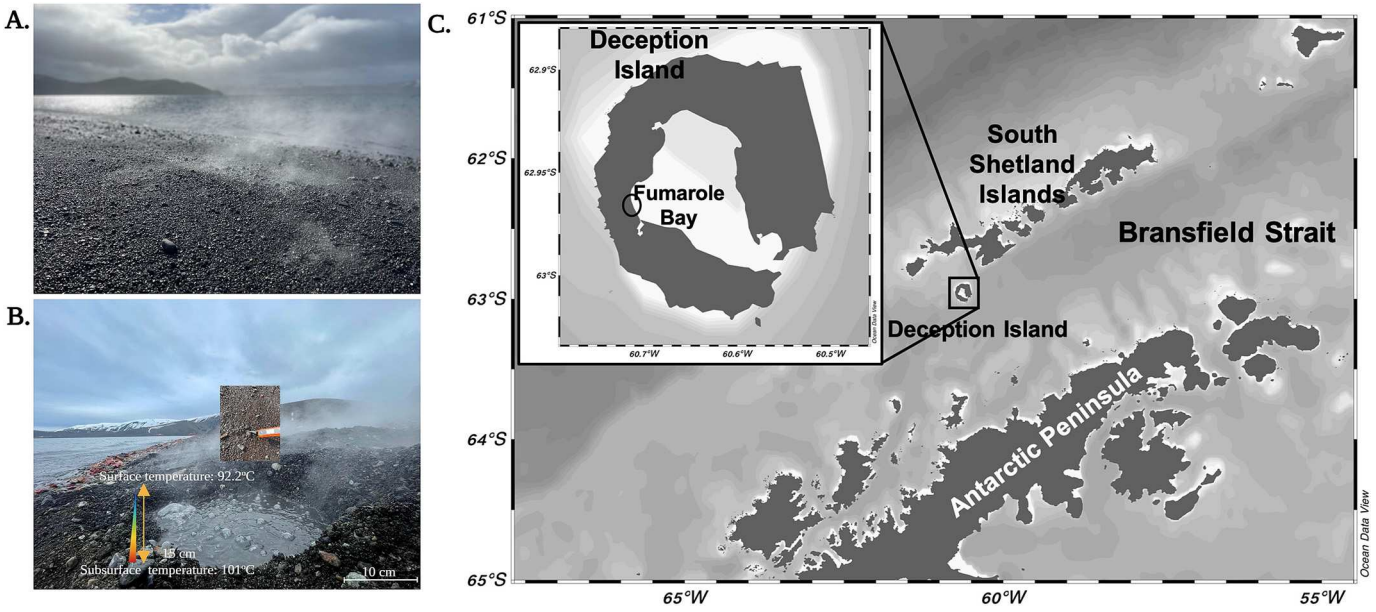

Fig. 1. A. Side view of the study site from a distance showing vapor **B.** Direct view of the study site showing the surface and sub-surface temperature **C.** Map showing the location of Fumarole Bay located on Deception Island, Antarctica.

containing Penicillin G (P) 10Unit, Clindamycin (CD) 2 μg, Co-Trimoxazole (COT) 25 μg, Erythromycin (E) 15 μg, Vancomycin (VA) 30 μg, and Ampicillin/Sulbactam (A/S) 10/10 μg; and lastly Hexa G-plus 15 containing Ciprofloxacin (CIP) 5 μg, Gentamicin (GEN) 10 μg, Linezolid (LZ) 30 μg, Penicillin-G (P) 10Unit, Streptomycin (S) 10 μg, and Vancomycin (VA) 30 μg spanning from the first to the fourth generation in a method previously described by Bauer et al. [37].

2.3. Taxonomic identification of EPS producing thermophilic bacteria by whole genome analysis

Genomic DNA from strain F2LB was isolated using DNA power soil kit (Sigma Aldrich) according to the manufacturer's instructions. DNA concentration and quality were assessed by using Nanodrop 1000 (Thermo Fisher Scientific) and Qubit 4.0 (Thermo Fisher Scientific). The genome sequencing was performed using Illumina Novaseq PE150 (Illumina, Inc., San Diego, CA, USA) platform using paired-end sequencing strategy. Raw reads were filtered, and high-quality paired-end reads were assembled using SPAdes (v3.15.5) [38]. CheckM was used to evaluate strain F2LB genome quality [39]. The identification of rRNA genes was carried out using RNAmmer (version 1.2) [40] and compared using the EzBioCloud server [41] and NCBI BLAST (https://blast.ncbi.nlm.nih.gov/Blast.cgi). The genome was visualized using Proksee [42] and compared with the closest species using BLAST [43]. Functional annotation and phylogenomic tree construction were performed using Anvi'o tool [44,45]. Prodigal was used to identify open reading frames [46], HMMER to identify genes matching bacterial single-copy core gene collections [47,48] and MUSCLE for multiple sequence alignment [49] and the resulting tree was visualized using MEGA (version 7.0) software [50]. Functional annotation was carried out against the Kyoto Encyclopedia of Genes and Genomes (KEGG) [51] database using the anvi-run-kegg-kofams program [52]. Pyani software package was used to calculate the average nucleotide identity (ANI) value [43,53]. Pangenome analysis was carried out using Roary [54] using the genome annotation by Prokka [55].

B. licheniformis F2LB genome was categorized in subsystem by using an open-source prokaryotic genome annotation system Rapid annotation System Technology (RAST) pipeline compared with the entire available dataset [56]. The functionally annotated genes present within the genome were visualized using SEED Viewer. PHAge Search Tool Enhanced Release (PHASTER) web-based server was used to identify genes related to prophage with the gnome of F2LB [57]. In order to predict genomic islands, IslandViewer4 was used (https://www.pathogenomics.sfu.ca/islandviewer/) [58].

Pan-genomes helped to estimate the number of shared genes (core genome) and unique or variable genes (accessory genome) between the genomes. The Spine tool (a perl-based program) was used to analyze the core genome from selected genomes with ≥85 % sequence identity as homologous [59]. AGEnt algorithm depends on a combination of the NUCmer function of the MUMmer software package v3.23 as well as the Perl script [60].

2.4. Analyzing the resistance under ultraviolet radiation

The growth pattern of isolated F2LB under UV exposure was checked by inoculating in both solid as well as liquid LB media and incubated for 24 h at 55 °C at dark condition. Inoculated plates and liquid media were subjected to UV-A and B radiation maintaining a 20 cm distance apart using a UV-LED light tube (Zcheng 5 W at 365–395 nm length) inside a LABWIT ZWYR-20102C shaker incubator. The exposure time gradually increased from 5 min (2.9 KJ/m^2), 10 min (5.9 KJ/m^2), 15 min (8.9 KJ/m^2), 20 min (11.9 KJ/m^2), 25 min (14.9 KJ/m^2), 30 min (17.9 KJ/m^2), 35 min (20.9 KJ/m^2) and 40 min (23.88 KJ/m^2). A non-irradiated plate and tube served as control. Bacterial growth was measured using Spectrophotometry at 590 nm.

To evaluate the cell viability and cell membrane integrity under UV radiation [61], the treated cells were then stained with LIVE/DEAD™ BacLight™ (Thermo Fisher Scientific, MA, USA). While SYTO 9 green only stains live cells, propidium iodide (PI) red stains dead or membrane damaged cells and extracellular DNA (eDNA). The stained cells were observed with a Leica Stellaris 5 confocal microscope (Leica Microsystems, Wetzlar, Germany) with excitation/emission for SYTO 9 of 485 nm/498 nm and PI of 535 nm/617 nm. Counts of the number of alive and dead cells have been performed using ImageJ software [62]. Cell viability % was calculated using the following Eq. (1)

$$\text{Cell viability } (\%) = \left[\frac{\text{NLive}}{\text{NLive} + \text{NDead}}\right] \times 100\% \quad (1)$$

where N_{Live} are the count of cells that are alive and N_{Dead} are the count of

dead cells

2.5. Formation of biofilm by isolated thermophilic B. licheniformis F2LB

Biofilm formation was done in Falcon tubes using 20 mL of growth medium and 200 μL of inoculum. Over a period of 6 days, we observed the growth of bacteria and the production of exopolysaccharides (EPS) from strain F2LB using confocal microscope (Leica Microsystems, Wetzlar, Germany). The sample was stained with DAPI (fluoresces at 358/461 nm) to visualize the bacterial cells, and SYPRO™ Ruby (fluorescence spectrum of 450/610 nm) to visualize the biofilm matrix.

Normalised mean fluorescence intensity also calculated from ImageJ using the following equation:

$$\text{Normalised mean fluorescence intensity (NMFI)} = \frac{MFI\ EPS}{MFI\ Biofilm} \quad (2)$$

where MFI EPS represented as mean fluorescence intensity of the EPS produced and MFI Biofilm represented as mean fluorescence intensity of the total biofilm produced

2.6. Recovery, production and OFAT optimization of EPS

The protocol described by Rimada and Abraham [63] was followed for production and recovery of EPS produced by *B. licheniformis* F2LB with little modification. Bacterial cell from stationary phase was treated with 4 % trichloroacetic acid (*w/v*) for 30 min followed by centrifugation at 5000 ×*g* for 20 min at 4 °C, 5000 ×*g* to precipitate the cellular proteins. An equal volume of solvent, acetone was added with the centrifuged supernatant and incubated at 4 °C for overnight. The solvent-coagulated EPS was centrifuged for 20 min (12,000 ×*g* at 4 °C) followed by lyophilization to obtain pure EPS powder. To determine the optimum nutrient source for the EPS production classical one-factor-at-a-time (OFAT) were executed where different nitrogen sources (casein hydrolysate, yeast extract and ammonium sulfate) and carbon sources (glucose, mannose, xylose and sucrose) were used. For experimental error stability, each experiment was performed in triplicate.

2.7. Physicochemical characterization of EPS

2.7.1. Morphological analysis of EPS (SEM-EDS and AFM)

To analyze the surface structure of the EPS, lyophilized samples were examined using scanning electron microscopy (SEM). To see the morphology of the sample under SEM, lyophilized EPS were fixed on aluminum stubs followed by making them conductive with the help of platinum coating, sputtered on samples. The platinum coating was 10 nm thick, and the platinum coated EPS sample was examined through Thermo Fisher Scientific Helios 5-CX focused ion beam-scanning electron microscope (FIB-SEM) (facility at South Dakota School of Mines and Technology, SD, USA), by maintaining an accelerated voltage of 5 kV. Elemental composition of the EPS sample was determined by Oxford UltimMax 100 EDS detector, and Oxford Symmetry S3 EBSD. The X-ray spectrum of the elements was obtained at an accelerating voltage of 15 keV. The sample was analyzed at 3 different locations with the varying magnification resolution of 2000×, 5000× and 10,000×. For the same location EDS was performed at multiple sites of the sample location to make the analysis more consistent.

To further analyze the morphological profile of the F2LB EPS, atomic force microscopy (AFM) measurements were conducted using the Anasys nanoIR3 system (Bruker, MA, USA), available at the South Dakota School of Mines and Technology (SDSM&T) facility in Rapid City, SD, USA. The sample was carefully prepared by sprinkling a small quantity of lyophilized EPS onto a double-sided sticky black carbon tape (5 mm in diameter) affixed to a mica substrate, ensuring adequate adherence and minimal contamination for precise imaging. The scanning was performed in tapping mode using a PR-EX-TNIR-D-10 probe with specifications included a radius of 20 nm, a spring constant of 40 N/m, a width of 40 μm, and an operational frequency of 300 kHz. The scan rate was maintained at 0.5 Hz to ensure high-resolution imaging, with areas of 5 × 5 μm and 20 × 20 μm analyzed at an X-Y resolution of 512 × 512 pixels. Before scanning, the probe was carefully engaged with the sample surface to achieve optimal interaction. During the scanning process, the setpoint amplitude was maintained at 7.281 V (target: 9 V) with a drive strength of 25.8 % at a resonance frequency of 167 kHz, allowing for stable imaging conditions without damaging the sample. The Anasys software suite was employed throughout the process, providing an intuitive interface for parameter configuration, data acquisition, and post-scan processing.

2.7.2. Monosaccharide composition analysis of the thermophilic EPS

To analyze sugar composition, five milligrams of EPS sample were added in 2M TFA acid and hydrolyzed at 120 °C for 90 min in a dry step. T-butyl-ethanol was added to the sample in cold conditions. The sample was vortexed and evaporated in an analytical evaporator with nitrogen gas at a temperature of 45 °C, and this step was repeated three times. Samples were diluted in deionized water and 0.45 μm filtered. Monosaccharide composition analysis was carried out using high-performance anion-exchange chromatography with a pulsed amperometric detector (HPAEC-PAD) using a DX 500 system (Dionex, Sunnyvale, CA, USA) equipped with a CarboPac PA10 column (250 × 4 mm). The analysis of neutral sugars was performed with water as the mobile phase (1 mL/min; 40 min), followed by a cleaning step with 300 mM NaOH for 10 min, and then 10 min of re-equilibration. Uronic acids were analyzed in 150 mM NaOH (1 mL/min; 30 min) using a 0–220 mM sodium acetate gradient, followed by a cleaning phase with 500 mM sodium acetate for 10 min, and a subsequent adjustment of 10 min with 220 mM NaOH and another 10 min with 150 mM NaOH. Standard monosaccharides used for this analysis included arabinose, fucose, galactose, glucose, mannose, rhamnose, and xylose, as well as uronic acids like galacturonic acid and glucuronic acid [64]. The experiment was performed in triplicates.

2.7.3. Determination of molecular weight

High-Pressure Size Exclusion Chromatography (HP-SEC) was executed to determine the molecular weight of the *B. licheniformis* F2LB EPS. Three milligrams of sample were weighed, and 1 mL of mobile phase ($NaNO_2$ 0.05 M and 0.02 % sodium azide) was used. The sample was vortexed for 1 min and treated for 1 min in an ultrasound water bath (Cole-Parmer8892, United States), until the samples were mixed. The sample was filtered with 0.05 μm PTFE Miller-LCR Merck (Agilent Technologies, United States) in a 1.5 mL glass tube. High-performance size-exclusion chromatography coupled with a refractive index detector (HPSEC-RID) was employed to assess the molecular weight distribution by using an Agilent 1250 Infinity system (Agilent, Santa Clara, CA, USA) equipped with a series of four PL aquagel-OH columns (60, 50, 40, and 30; 300 × 7.5 mm) arranged in tandem (Agilent, Santa Clara, CA). The mobile phase was delivered at a flow rate of 0.6 mL/min, with the RID temperature set to 30 °C. The average molecular weight (Mw) of samples was determined using a dextran standard curve (Mw 5, 12, 25, 50, 80, 150, 270, 410, 670 kDa; Sigma-Aldrich, St. Louis, MO, USA). The void volume (Vo) corresponded to the elution time of the largest molecule while the included volume (Ve) matched the elution time of glucose [64]. The slope for calculating the Mw of the samples was derived from the log-transformed dextran standard curve, described by the equation: $y = -51{,}968\times + 66{,}188$ ($R^2 = 0{,}9976$). The experiment was carried out in triplicates.

2.8. Determination of thermal stability

For analyzing thermal stability, a microprocessor driven temperature-control incorporated thermogravimetric analyzer Cahn-Ventron 2000 (Cahn Scientific, Irvine, CA, USA) was used. 5 mg of EPS sample was weighed in an aluminum pan, then the experiment

performed under 50 mL/min N_2 gas flow, at a heating rate of 10 °C min^{-1} where temperature gradually increased from 25 to 600 °C.

2.9. Determination of surface area

Brunauer-Emmett-Teller (BET) surface area analysis was performed using a Micromeritics Gemini III 2375 Specific Surface Area Analyzer at South Dakota School of Mines to determine the specific surface area of the EPS sample. Ultra-high purity (UHP) nitrogen gas was used as an adsorbate, while UHP helium gas was utilized to measure the free space within the sample cell. Prior to analysis, approximately 0.205 g of the sample were placed in the sample holder and degassed under a continuous flow of UHP nitrogen gas at room temperature to remove any physically adsorbed contaminants or moisture. The degassing process was conducted for 6 h to ensure complete removal of volatiles and achieve a stable baseline. During the measurement process, nitrogen adsorption and desorption isotherms were recorded over a relative pressure (P/P_o) range of 0.05 to 0.95. The specific surface area was calculated using the BET equation, assuming a monolayer coverage of nitrogen molecules on the surface. All measurements were conducted at controlled room temperature to minimize fluctuations due to environmental conditions. The instrument was calibrated to ensure accuracy and reproducibility of the results.

2.10. Putative EPS backbone structure analysis by spectroscopic study

2.10.1. Determination of functional groups by Fourier transform infrared (FTIR) spectroscopy

Fourier transform infrared spectroscopy was performed to analyze the main functional groups of the studied thermophilic EPS. Around 5 mg sample was analyzed in absorbance mode in a FTIR-ATR spectrometer (Bruker Alpha Platinum-AIR, USA) with a scan range of 4000–400 cm^{-1} where crystal was placed at a 45° angle and 64 scans were executed (4 cm^{-1} resolution). Opus 8.1 Software was used to process the spectra.

2.10.2. Analysis of glycosidic linkages by HSQC-NMR spectroscopy

Nuclear magnetic resonance (NMR) analysis followed established protocols. A sample of 20 mg of *B. licheniformis* F2LB exopolysaccharide was examined using a 500 MHz NMR spectrometer (Bruker Biospin, Rheinstetten, Germany) equipped with a triple resonance probe [64,65]. The sample was dissolved in 99.9 % deuterium oxide (Cambridge Isotope Laboratory, Cambridge, MA). $^{1}H/^{13}C$ Multiplicity-Edited HSQC spectra were obtained with 1024 × 512 points and 256 scans, utilizing an Echo-Antiecho acquisition method and globally optimized alternating phase rectangular pulses for decoupling at 35 °C. The spectra were processed using TopSpin 4.3.1 software (Bruker Biospin). Chemical shifts were compared manually with the Carbohydrate Structure Database (CSDB) [66] and relevant literature to identify likely glycosidic linkages [67].

2.11. Functional property elucidation of the EPS

2.11.1. In vitro antioxidant activity determination

The free radical scavenging activity was assessed using the method of Ruch et al. [68], with slight modifications. The primary reaction mixture was prepared by mixing EPS samples of various concentrations (1, 2, 3, 4, and 5 mg mL^{-1}) in 50 μL volumes and 120 μL of 0.1 M phosphate buffer (pH 7.40) and 30 μL of 40 mM H_2O_2 solution was added to each primary reaction mixture. The final reaction mixtures were thoroughly shaken and incubated at 30 °C for 10 min. Then, the absorbance of each sample was measured at 230 nm using a microplate reader (Allsheng, Flex A-200, China). The H_2O_2 scavenging activity was then calculated using the appropriate eq.

$$[1-(A_1-A_2)/A_0]\times 100 \quad (3)$$

where A_0 is distilled water absorbance, A_1 is a sample water absorbance mixed with H_2O_2, A_2 is the sample water absorbance.

The radical scavenging activity (RSA) of 2,2-diphenyl-1-picrylhydrazyl (DPPH) was determined following the methods given by Shimada et al., [69] with some adjustments. In summary, different concentrations of 200 μL of EPS aqueous solution (1, 2, 3, 4 and 5 mg mL^{-1}) were mixed with 20 μL (0.2 mM) ethanolic DPPH solution. The mixture was then kept in the dark at 30 °C for 1 h and subsequently centrifuged at 5000 ×*g* for 10 min. The absorbance of the supernatant was measured at 517 nm using a microplate reader (Allsheng, Flex A-200, China). The following equation was used to calculate the DPPH scavenging activity:

$$[(A-B)/A]\times 100 \quad (4)$$

where A is the absorbance of control supernatant and B is the absorbance of the sample respectively

The determination of Ferric Reducing Antioxidant Power (FRAP) activity was carried out following the method established by Benzie and Strain [70] with certain adjustments. The EZAssayTM (Antioxidant Activity Estimation Kit, Himedia, India) was utilized for the FRAP assay, with the addition of 100 μL of chromogenic substrate and 100 μL of the sample. The mixture was then incubated in darkness for 10 min at room temperature (25 °C). The absorbance of the mixture was measured at 560 nm using a microplate reader (Allsheng, Flex A-200, China). The standard calibration curve was prepared using different concentrations of ferrous standard provided in the kit. Fe (II)iron equivalents (μM) were calculated using the following equation:

$$A=\frac{b\,(x\times y)}{c} \quad (5)$$

where A is Fe^{2+} (μM), B is absorbance, (x-y) intercept and C slope. Xanthan gum was used as positive control here.

To assess the chelating activity of ferrous metal ions based on the methods given by Shi et al. [71], aqueous samples were prepared at various concentrations. For each sample, 100 μL of the sample, 10 μL of 2 mM $FeCl_2$, and 40 μL of 5 mM ferrozine were added. Negative control was established by replacing the sample with H_2O, while H_2O was used instead of 2 mM $FeCl_2$ to create a sample with no activity. In this study, EDTA served as the positive control. After incubating the test set in darkness for 10 min at 37 °C, the absorbance of the samples was measured at 562 nm using a spectrophotometer. The % Fe^{2+} chelation was calculated according to the following equation:

$$[1-(A_1-A_2))/A_0]\times 100 \quad (6)$$

2.11.2. Analysis of emulsification activity

The emulsifying activity of EPS produced by *B. licheniformis* F2LB was performed using the method discussed before by Cooper and Goldenberg [72], with some adjustments. To execute the emulsifying activity, edible vegetable oils were utilized, including sesame, sunflower, canola, olive, corn, grape seed, vegetable, and rice oil. The emulsifying property of the EPS compared with commercially available bacterial polysaccharide xanthan gum (Sigma, St. Louis, Missouri, USA). For this experiment, 2 mL of an aqueous solution of our studied EPS (1 mg mL^{-1}) were added, followed by 3 mL of each vegetable oil (2:3 v/v). The mixture was vigorously stirred for 2 min. The oil, emulsion, and aqueous layers were measured at 24-hour intervals to evaluate emulsion stability. All experiments were performed in triplicate. The emulsification index (E_{24}) was calculated using the following equation:

$$\left[\left(\text{volume of the emulsion layer}\times \text{total volume}^{-1}\right)\times 100\right] \quad (7)$$

2.12. Water-holding and oil-holding capacity determination

The water-holding capacity (WHC) of the EPS produced by *B. licheniformis* F2LB was determined by method described before by

Kumari et al. [73] in triplicates with little modification. 500 mg of purified EPS was mixed with 10 mL of distilled water by vortex for 1 min. The mixed solution was kept in rest for 30 min with intermediate stirring occasionally. Then the reaction mixture was centrifuged at 3200 rpm for 25 min and the supernatant was discarded. Then the weight of the EPS was taken to calculate the water-holding capacity (WHC) using the formula:

$$\%WHC = [Water\ bound\ weight\ (g)/Initial\ sample\ weight\ (g)\,] \times 100 \quad (8)$$

The oil-holding capacity (OHC) of the studied EPS of *B. licheniformis* F2LB was determined by method described before by Wang and Kinsella [74] in triplicates with little modification. 500 mg of EPS was mixed with 10 mL of sunflower oil by vortex for 1 min. The mixed solution was kept in rest for 30 min with intermediate stirring occasionally. Then the reaction mixture was centrifuged at 3200 rpm for 25 min and the supernatant was discarded. Then the weight of the EPS was taken to calculate the oil-holding capacity (OHC) using the formula:

$$\%OHC = [Oil\ bound\ weight\ (g)/Initial\ sample\ weight\ (g)\,] \times 100 \quad (9)$$

2.13. Statistical analysis

Graphpad Prism version 10, OriginPro 2018, and Biorender were utilized for graphical representations and statistical analysis. Every data point represents mean ± SD. Additionally, descriptive statistics have been performed for the physicochemical characterization of the study site and the EPS's water/oil holding activity. One-way ANOVA (Bonferroni test) was performed for pH, Salinity, antibiotic, and UV exposure on bacterial colony size determination assay, biofilm production, cell surface area, and EDS analysis of the EPS with the Bonferroni multiple comparison test. Two-way ANOVA (Bonferroni test) was performed for antioxidant activity determination and emulsification test, as in these cases, the group sizes were unequal.

3. Results

3.1. Study site, sample collection and in-situ analysis

The physicochemical characterization of the thermal anomalies of interstitial water found in the intertidal coastal marine zone in Fumarole Bay is summarized in Table 1. A map of the study site is presented in Fig. 1. Marine waters (35.03 ± 3.27), slightly acidic (pH 5.69 ± 0.36), and extremely hot (99.97 ± 0.12 °C) dominated the system. In addition, compared to other thermal anomalies present along the coast (data not shown), relatively high oxidative conditions (Oxidation-Reduction Potential (ORP) 132.3 ± 10.41 mv) were found. Although low concentrations of total dissolved solids (28.13 ± 2.58 ppt) were registered, electrical conductivity was relatively high (56.3 ± 5.14 mS cm^{-1}). On the other hand, there was a low availability of phosphates (0.25 ± 0.03 μM) and hydrogen sulfide (0.14 ± 0.06 μM), while silicates were relatively high (487.06 ± 7.61 μM). Furthermore, in contrast to N_2O (11.4 ± 0.80 nM) and CH_4 (12.3 ± 0.80 nM), CO_2 concentrations (1277.8 ± 75.80 μM) were extremely high. At the moment of the sampling, UV (UVA + UVB) radiation was 637.33 ± 6.66 μW cm^{-2}. The descriptive statistics results of the parameters are detailed in Table S1.

3.2. Isolation and polyphasic characterization of the EPS producing thermophilic bacteria

Growth of numerous thermophiles had been observed on LB media at 55 °C. The F2LB strain was initially isolated from these thermophilic colonies as a white, opaque, circular, and undulate colony with a length of approximately 5.25 mm, which caught our attention due to its colony size and time of growth. The strain was subsequently optimized for cell growth under varying salt concentrations and pH conditions. It was observed that bacterial cell growth was maximum at pH 7 and with 2 % salt concentration (Supplementary Figs. S1 and S2). When pairwise comparison was performed using one-way ANOVA through Bonferroni's multiple comparison tests between the pH groups, it was observed that the culture at pH 7 showed an extremely significant increase in bacterial density compared to the other pH ranges ($p < 0.0001$); in turn, these showed highly significant differences among themselves ($p < 0.0001$), except between pH 6 and 5 (Table S2). Cultures with 1 % and 2 % salt concentrations recorded similar and higher absorbances than the other concentrations used. Moderately significant differences were found between these cultures and those with 5 % salt concentrations ($p < 0.01$). Significant differences were observed between cultures with 1–2 % salt concentrations and cultures with 3–4 % salt concentrations ($p < 0.05$). (Table S3). The cellular growth was optimum at pH 7 and a 1–2 % NaCl concentration. Then, EPS production was executed to analyze these isolated colonies further downstream. Fumarolic isolate F2LB was found to be susceptible to all tested antibiotics from the first to the fourth generation, which indicates primarily that the bacteria have been in an isolated extreme environment devoid of possible events of horizontal gene transfer. Broad-spectrum antibiotic sensitivity profiling of the isolate F2LB was statistically standardized using one-way ANOVA and Bonferroni's multiple comparison test (Figs. S3 and S4). Nalidixic acid showed the lowest antibiotic effect against *B. licheniformis* F2LB with moderately significant differences versus inhibition with ciprofloxacin, amikacin, netillin, and ofloxacin, which were given the most prominent inhibition ($p < 0.01$). Also, it was observed that F2LB cultures showed a lower sensitivity to clindamycin among the other antibiotics, with significant differences when Ampicillin/Sulbactam, Gentamicin, Linezolid, and Vancomycin were used ($p < 0.01$). It has been observed that the pairwise group combinations have significant differences with $p < 0.05$ and $p < 0.01$ (Tables S4 and S5). The zone of inhibition was found to be the lowest in the case of the first-generation antibiotic nalidixic acid. However, the zone of inhibition was found to be highest in the case of ciprofloxacin, a second-generation antibiotic.

Table 1
Average (± Standard Deviation) of physicochemical parameters measured in situ and from samples taken from the interstitial waters with highest thermal anomaly (at 30 cm depth approx.) found in the coastal marine intertidal zone of Fumarole Bay.

Station	Position		In situ measurements							
	Latitude	Longitude	pH	Temperature (°C)	EC (mS cm^{-1})	Salinity (%)	Salinity (ups)	TDS (ppt)	ORP (mV)	UVA + UVB (μW cm^{-2})
Fumarole bay	62°58′6.1″S	60°42′32.7″W	5.69 ± 0.36	99.97 ± 0.12	56.30 ± 5.14	3.46 ± 0.33	35.03 ± 3.27	28.13 ± 2.58	132.33 ± 10.41	637.33 ± 6.66
			Inorganic compounds					GHG		
			Nitrate (μM)	*Nitrite (μM)*	*Phosphate (μM)*	*Silicate (μM)*	*Hydrogen Sulfide (μM)*	*CO_2 (μM)*	*CH_4 (nM)*	*N_2O (nM)*
					0.25 ± 0.03	487.06 ± 7.61	0.14 ± 0.06	1277.8 ± 75.8	12.3 ± 0.80	11.4 ± 0.80

*EC = Electric conductivity; TDS = Total Solids Suspended; ORP = Oxidation Reduction Potential; GHG = Greenhouse Gases.

3.3. Taxonomic identification of EPS-producing thermophilic bacteria by whole genome analysis

The 16S rRNA gene sequence (extracted from the F2LB genome) showed 100 % identity to the type strain of *Bacillus licheniformis* based on pairwise digital DNA-DNA hybridization (dDDH) values between user genomes and selected type strain genomes. Table S6 includes dDDH values along with their confidence intervals. In the phylogenomic tree (Fig. 2A), strain F2LB clade with *Bacillus licheniformis.* The ANI value between F2LB and *B. licheniformis* was 99.5 %. Therefore, the isolated strain has been identified as *B. licheniformis* F2LB. The morphological characteristics indicate a rod-shaped bacterial cell (Fig. 2B–C). The genome size of *B. licheniformis* F2LB was 4,248,298 bp with 46.2 % GC content. The genome completeness was 98.8, with 0.4 contamination. The circular visualization and its comparison with *B. licheniformis* DSM 13 are depicted in Fig. 2D. The genome sequence was submitted to GenBank under the accession number JBFNAG000000000.

B. licheniformis F2LB encodes genes for glycolysis, citric acid cycle and pentose phosphate pathway. It also encodes genes for dissimilatory nitrate reduction (*NarGHI and NirBD*), assimilatory sulfate reduction (sat, cysc, cysH and cysJI), and biosynthesis of ornithine, arginine, proline, tryptophan, riboflavin, and betaine. F2LB encodes genes to overcome stress UV irradiation (uvrABCD), cold and heat shock (cspA, htpX, htpG, hslO, dnaJ, dnaK, and grpE). *B. licheniformis* F2LB encodes genes for the uptake of glucose, galactose, fructose, sucrose, maltose, mannose, xylose, arabinose, lactose, trehalose and cellobiose. Gene related to the biosynthesis of UDP-*N*-acetyl-D-glucosamine biosynthesis (glk, gpi, glmS, glmM and glmU), nucleotide sugar (glk, pgm and galu) and EPS production (epsA, epsB, epsD, epsE, epsF, epsG, epsM and epsN) were observed in *B. licheniformis* F2LB genome. The metabolic pathway for EPS production by F2LB had been predicted in Fig. 3 based on the supplementary information .csv file. F2LB genome was analyzed for the presence of prophage sequenced by using PHASTEST, a web-based PHAge search tool [57]. It identified three annotated regions for the presence of prophage (Fig. 4). The phages with the highest number of proteins, most similar to those in the region, the three most common phages have been predicted, PHAGE_Bacill_phi105_NC_048631, PHAGE_ Bacill_WBeta_NC_007734 and PHAGE_Brevib_Jimmer1_NC_029104 which is provided on Fig. 4. The blast hits to identify the phages have been detailed in Table S7. Genomic islands (GIs) mainly consist of foreign genetic material acquired by horizontal gene transfer [58]. In total, 8 GIs (Fig. 5b) were predicted to contain genes required for cell metabolism, EPS biosynthesis, and more. GI-8 contains heavy metal translocating P-type ATPase, a polysaccharide biosynthesis protein, which confirms the EPS production by the bacteria. Apart from this, GI-2 and GI-7 contained the prophage-related gene present in *B. licheniformis* F2LB. Pangenome analysis of *B. licheniformis* F2LB was carried out between two closely related *Bacillus* species (Fig. 2E). A total of 6027 gene clusters were noticed and the Venn diagram (constructed using the presence and absence of genes) showed that *B. licheniformis* F2LB consists of 149 unique genes compared to *Bacillus paralicheniformis* KJ-16 and *Bacillus licheniformis* DSM 13 (Fig. 2F–G). The relative distribution of pan, core, and accessory genome of F2LB according to the subcategory and the total number of genes is provided in Table S8. The GI start and end length and the gene products present in each genomic island have been provided in Table S9.

3.4. Analyzing the resistance of the ionizing radiation

F2LB was capable of tolerating 35 min (20.9 KJ/m^2) of gradually increasing UV-B exposure (Fig. 6A). However, after this level, at 40 min (23.88 KJ/m^2) UV-B exposure, the growth of F2LB was null. The colony morphology of the treated cell was significantly larger than the control one (without exposure). The colony exposed for more time to UV found to be dry, flattened, and bigger (Fig. S5). On the other hand, the colony without UV exposure is found to have mucoid, small convex colony morphology. This indicates that the cells stop producing EPS when exposed to UV radiation. From Fig. 6, it can also be clearly found that the growth intensity of F2LB was the same however the cell morphology changed. Moreover, cells were likely to form aggregation within the population of UV-treated *B. licheniformis* F2LB. Confocal micrograph of the treated *B. licheniformis* F2LB found to have chain-like formation indicating the biofilm synthesis at stress condition. Under controlled UV exposure, cell viability % gradually decreases from 47 % at 5 min to 15 % at 40 min. The highest cell viability percentages have been observed at 10 min (51 %), whereas for control, 55 % cell viability has been observed where no UV exposure has been applied (Fig. S5A). The highest colony size was observed at 25 min UV exposure (~6.8 mm). It gradually increases from 3.6 mm at 5 min to 6.8 mm at 25 min under UV exposure (Fig. S5B and C). Upon statistical analysis through one-way ANOVA pairwise comparison test, growth inhibition under controlled UV exposure at different time lapses is presented in Fig. S6. Additionally, a pairwise comparison of each UV exposure group was obtained using one-way ANOVA Bonferroni's multiple comparisons test, which is detailed in Table S10. UV-resistant related DNA repair genes identified from the genome of *B. licheniformis* F2LB have been presented in Table S11.

3.5. Formation of biofilm by thermophilic B. licheniformis F2LB

Biofilm formation is a successful strategy for microorganisms to survive in a hostile environment [75]. The formation of biofilm by this bacterium was analyzed using confocal microscopy to confirm the formation of biofilm by thermophilic *B. licheniformis* F2LB. Fig. 6B indicates the production of a higher number of planktonic cells during the initial days (1 day and 2 days). However, biofilm production increased significantly until day 4 and then declined until day 6. The biofilm coverage area observed by microscopy on day 4 showed significant differences compared to those produced on days 2 and 5, significantly different from those produced on the remaining days ($p < 0.001$). Moreover, Fig. 6 depicts that F2LB started to produce biofilm after 24 h from inoculation. Normalised mean fluorescence intensity from the confocal micrograph of the biofilm produced by *B. licheniformis* F2LB also provide the insights that this bacterial strain produced highest of extracellular polymeric substances after 4th day which gradually decreased later on (Fig. S7). Pairwise comparison between biofilm production over time, using one-way ANOVA with the Bonferroni Multiple Comparison test, proves the statistical significance of the experiment, as may be observed in Fig. S8 and Table S12. Additionally, the percentage of cell surface area of F2LB was studied with a pairwise comparison between biofilm production over time employing one-way ANOVA with Bonferroni Multiple Comparison (Fig. S9 and Table S13). Similar to what was observed with biofilm production, the area covered by cells in the culture increased until reaching a maximum on days 3 and 4. These differences were moderately significant compared to the other cultures ($p < 0.01$). A notable decrease in the bacterial density of the culture was observed on day 6, with a significant reduction compared to the maximum recorded on days 3–4 ($p < 0.0001$). In the present study, being exposed to high temperatures, F2LB was found to produce biofilm to survive in extreme environmental conditions. This also confirms the production of a dense mass of extracellular polymeric substances, which help microbial cells serve a protective function [5].

3.6. Recovery, production, and OFAT optimization of the thermophilic EPS

In the stationary growth phase, at 55 °C, the highest EPS production was observed by *B. licheniformis* F2LB when the trichloroacetic acid precipitation method was executed [5]. The best-optimized nitrogen source was yeast extract, resulting in the initial EPS production of 0.43 g L^{-1} in pre-optimized conditions. The highest yield was 0.992 g L^{-1}, where the best-optimized nitrogen source was yeast extract, pH was 7,

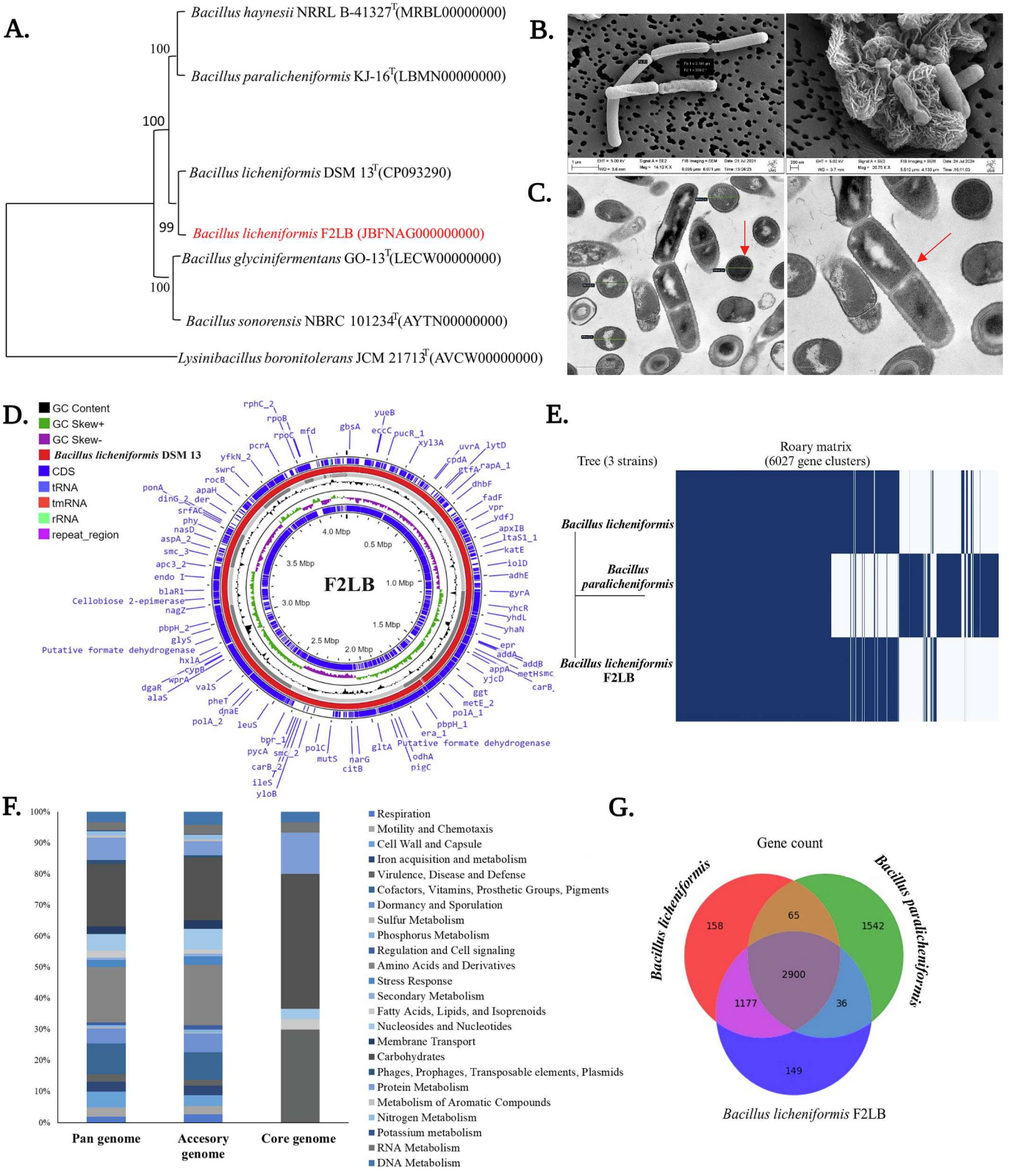

Fig. 2. **A.** The maximum likelihood phylogeny of isolate F2LB shows similarity with *Bacillus licheniformis*. **B.** SEM micrograph demonstrating the morphology and the size (2.191 μm) of the isolated F2LB. **C.** TEM micrograph demonstrating the endospore formed by the cell (marked with red arrow) and 2D projection of the dividing cell (marked with green arrow). **D.** Circular representation of annotated whole genome of *Bacillus licheniformis* F2LB created using Proksee. **E.** Roary gene cluster, showing the presence and absence of genes. **F.** Relative distribution of pan, core, and accessory genome through Spine and Agent tool, where each category or subcategory is plotted as a percentage of the total number of genes. **G.** Venn diagram (based on presence and absence of genes) between *Bacillus licheniformis* F2LB and the other two closely related *Bacillus* species. Raw data provided in supplementary materials (Table SXX).

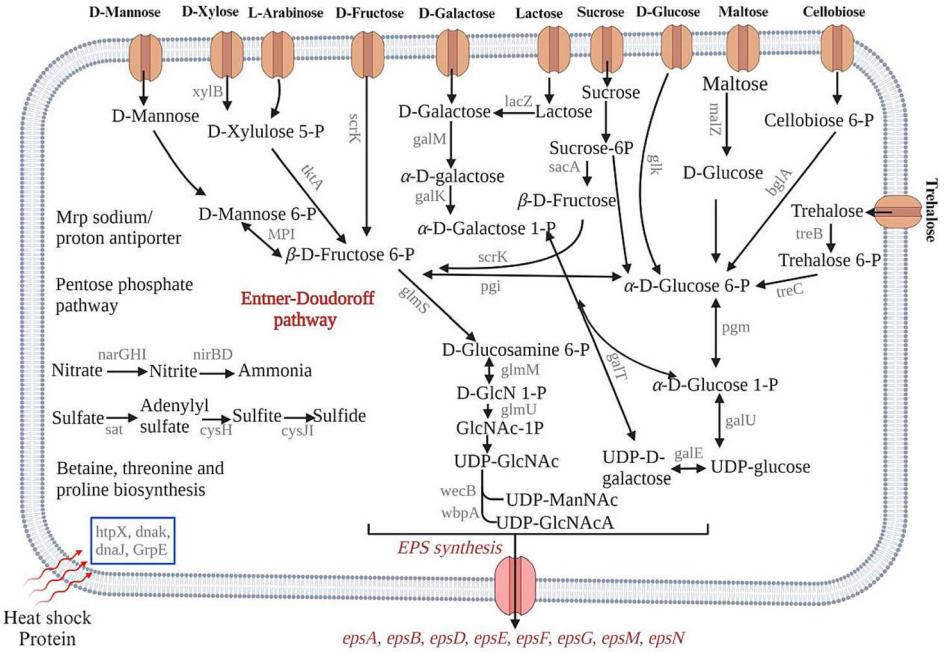

Fig. 3. Predicted metabolic pathways of *Bacillus licheniformis* F2LB based on KEGG (Kyoto Encyclopedia of Genes and Genomes) databases. The dashed line arrow indicates the absence of the gene.

and NaCl concentration was 2 %.

3.7. Physicochemical characterization of EPS

3.7.1. Morphological analysis of EPS (SEM-EDS)

SEM was performed at 2000×, 5000×, and 10,000× magnification in 3 different sites to understand our studied EPS's three-dimensional structure and surface morphology. It was observed that *B. licheniformis* F2LB EPS had a compact surface with a nonporous and rough structure (Fig. 7A). Upon further magnification, it was found that roughness was mainly due to the presence of dispersed, undulated macromolecular lumps. Similar kinds of EPS structures had been found before by Hu et al., [76] for a *Planococcus rifietoensis* isolated from deep-sea sediments of the Northwest Pacific and Gan et al. [77] for the halophilic strain of *Halomonas saliphila*. Both are of marine origin, producing EPSs of high molecular weight and excellent thermal stability. However, the morphology of the biopolymer may differ according to the isolation and extraction procedure along with the physicochemical properties [78]. EDS micrograph revealed that this heteropolymer is mainly made of carbon, oxygen, and phosphorus with 41.88, 18.64, and 14.98 % of its total weight respectively along with the atomic weight of 60.43, 20.24, and 8.38 % respectively (Fig. 7B). Presence of trace amount of nitrogen (weight% 1.19, atomic% 1.48) and sulfur (weight% 0.49, atomic% 0.26) indicates a low chance of having protein residues and other undesired contaminants in the extracted EPS. In the F2LB EPS, phosphorus (P), carbon (C), and oxygen (O) exhibited the highest % of total weight compared to the other detected elements. Significant differences were observed in the levels of C and O relative to the remaining elements ($p < 0.001$), except for sodium (Na), calcium (Ca), and phosphorus (P) where moderately significant differences were observed when compared to the content of the other elements ($p < 0.01$). The elemental composition of the EPS is statistically significant, as may be observed from one-way ANOVA with Bonferroni Multiple Comparison with a minimum value of $p < 0.001$ (Fig. S10 and Table S14).

The AFM analysis of the F2LB EPS (Fig. 7C and D) revealed a highly heterogeneous surface morphology, distinguished by significant height variations and intricate topographical features. Quantitative analysis of the 5 × 5 μm region (Fig. 7C) identified a peak-to-valley height difference of 255 nm, underscoring substantial topographical heterogeneity across the scanned area. Complementary 3D topological mapping of a larger 20 × 20 μm region (Fig. 7D) further highlighted the morphological complexity, with localized height fluctuations ranging from approximately −40 nm to +30 nm. These observations were reinforced by an RMS roughness value of 74.54 nm, reflecting the overall surface texture and irregularity. The height distribution (profile analysis) demonstrated a broad spectrum of intensity values, with a notable concentration around mid-level heights. This suggests a composite surface architecture comprising prominent elevated features interspersed with smoother, recessed regions. Such morphological characteristics point to a highly textured and structurally diverse EPS matrix. The roughness (Ra), skewness (Rsk), and kurtosis (Rk) values of the AFM data for the extracted EPS are presented in supplementary information as mean values, supported by the standard deviation in triplicates. The observed Ra, Rsk, and Rk of the EPS matrix analyzed over varying scan sizes (5 × 5 μm^2, 10 × 10 μm^2, and 20 × 20 μm^2) provide insights into the molecular interactions and structural organization dictated by the EPS's compositional and molecular weight diversity (Supplementary Table S15). The Ra increased from 10.07 ± 2.52 nm at the smallest scan area to 22.94 ± 3.43 nm at the largest, indicating that the EPS forms increasingly complex and textured surface morphologies at higher resolutions. The Rsk values, ranging from −0.818 ± 0.071 to −0.298 ± 0.024, suggest a predominance of valleys over peaks in the EPS surface topology, reflecting the potential for molecular entrapment and interaction. Moreover, the Rk values (3.204 ± 0.66 to 4.57 ± 0.97) indicate surface features with sharper height distributions, which are conducive to the EPS's functional properties, such as enhanced surface adhesion and biofilm formation. The observed roughness and complex topography are likely indicative of underlying molecular interactions, including polymeric arrangement and compositional heterogeneity. These findings suggest that the EPS exhibits a strong tendency to form structured aggregates, which may enhance its functional properties, such as surface adhesion, structural integrity, and bioactivity.

3.7.2. Monosaccharide composition analysis of the thermophilic F2LB EPS

Liquid chromatography unveiled (Fig. 8A) the composition of the exopolysaccharide macromolecules, which were mainly composed of

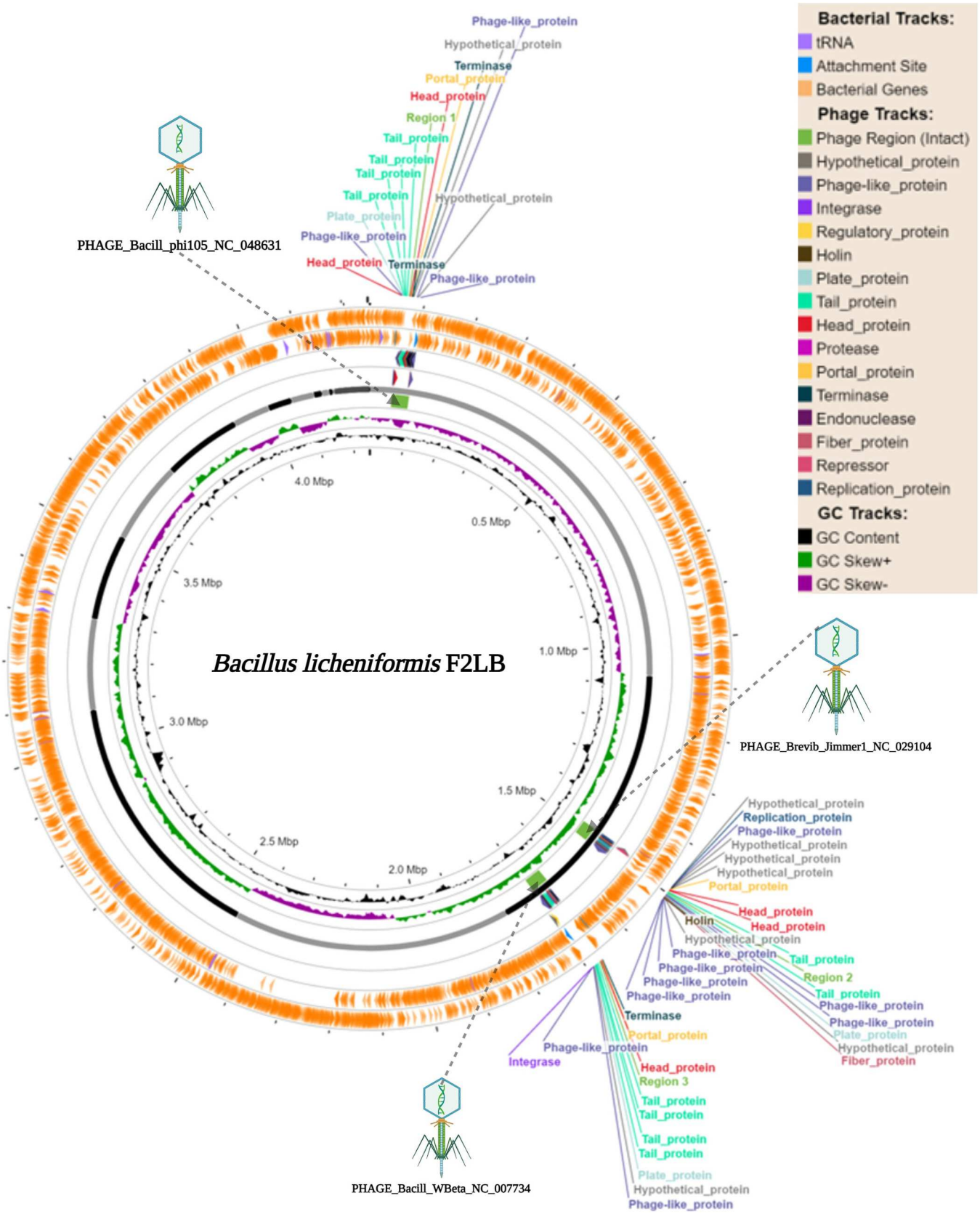

Fig. 4. Circular genomic map of *Bacillus licheniformis* F2LB obtained from PHASTEST.

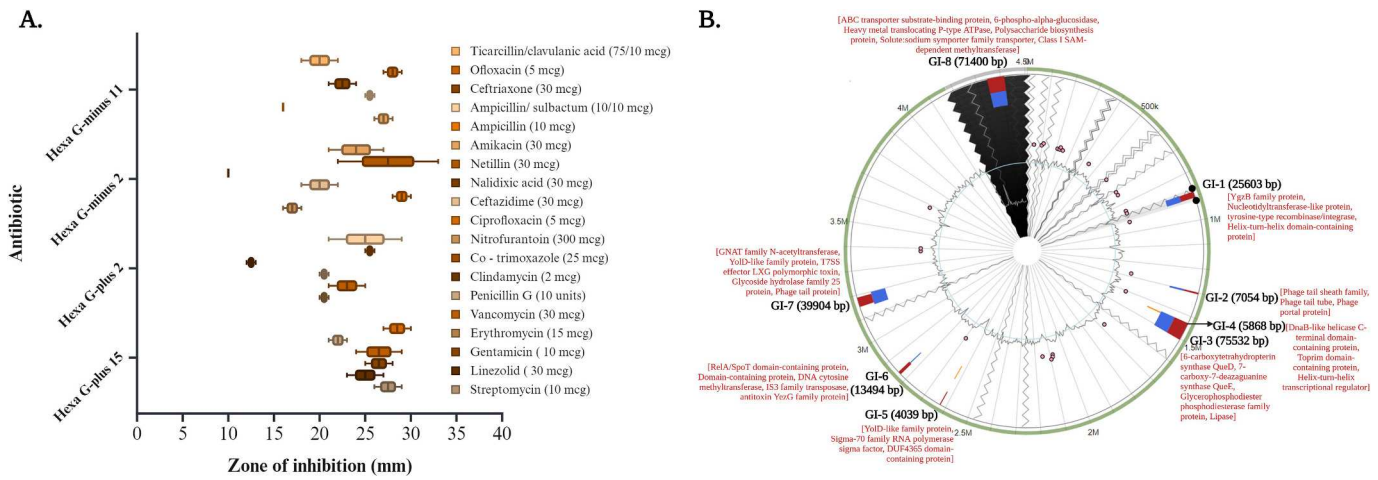

Fig. 5. A. Antibiotic resistance analysis of *Bacillus licheniformis* F2LB, **B.** Demonstrating Genomic Islands predicted from the genome of *Bacillus licheniformis* F2LB.

mannose (1.595 ± 0.253 μg/ 25 μL), glucose (1.112 ± 0.227 μg/ 25 μL), xylose (0.590 ± 0.189 μg/ 25 μL), fucose (0.421 ± 0.074 μg/ 25 μL), arabinose (0.081 ± 0.115 μg/ 25 μL), and galactose (0.067 ± 0.027 μg/ 25 μL), with some minor other sugars. The molar ratio was Man: Glu: Xyl: Fuc: Ara: Gal (1: 0.7: 0.4: 0.3: 0.05: 0.04). Mannose, glucose, and xylose represent the predominant monosaccharides in the EPS-F2LB matrix with the highest mol%, exhibiting statistically highly significant differences in their concentrations compared to arabinose, galactose, galacturonic acid, glucuronic acid, and rhamnose ($p < 0.0001$). Furthermore, substituents such as galacturonic acid (0.028 ± 0.002 μg/ 25 μL) and glucuronic acid (0.028 ± 0.002 μg/ 25 μL) had been observed. No traces of rhamnose were found. No other monosaccharides were detected using this method. Also, monosaccharide composition has been studied with one-way ANOVA with Bonferroni Multiple Comparison, where $p < 0.0001$ (Fig. S11 and Table S16).

3.7.3. Determination of molecular weight

HPSEC revealed that Deception Island isolated *B. licheniformis* F2LB produced two sets of EPS fraction (Fig. 8B), one from high to medium distribution (516 KDa to 8 KDa), and another as low molecular weight (below 5 KDa). This is the first clue about the complexity of exopolysaccharides produced by the microorganism that could make it more adapted to high temperatures.

3.8. Determination of thermal stability

Thermogravimetry was used to evaluate the thermal stability of EPS from *B. licheniformis* F2LB. Fig. 8C displays this polysaccharide's TG and DTG curves, while Table 2 presents the analysis results (supplementary. csv_2). Fig. 8C shows that the EPS thermogram has three distinct thermal effects. The first occurs between 25 and 165 °C, with a T_{peak} of 90 °C and a mass loss of 17.2 %. This effect corresponds to the evaporation of free and bound water from EPS [5]. Similar weight loss (17 %) was observed for EPS from *B. licheniformis* PASS26, but the T_{peak} (100 °C) associated with this process was higher [79]. The second pyrolysis stage occurs between 166 and 293 °C and reaches its maximum decomposition rate at 255 °C. This process is linked to the pyrolytic breakdown of EPS and results in a mass loss of 21.3 %. At this point, volatile chemicals are released due to the hydrolysis and ring dehydration of the polymeric chains [5]. Finally, a third effect has a peak temperature of 328 °C, occurring in a temperature range of 294–435 °C, and has a mass loss of 13.8 %. This is due to residual polysaccharide decomposition.

3.9. Determination of surface area

The BET surface area of the sample was determined to be 1.0795 m^2/g, while the Langmuir surface area was slightly higher at 1.7597 m^2/g, indicating the presence of microporous structures. The single-point surface area at P/Po = 0.2502 was 0.9373 m^2/g. The cumulative surface area of pores within the 17–3000 Å diameter range, as determined by the Barrett-Joyner-Halenda (BJH) adsorption method, was 0.7403 m^2/g. The total pore volume of pores smaller than 410.4 Å, measured at P/Po = 0.9508, was 0.001347 cm^3/g, with a BJH cumulative pore volume of 0.001093 cm^3/g. The adsorption average pore diameter calculated using the 4 V/A BET method was 49.91 Å. In comparison, the BJH adsorption average pore diameter was slightly larger at 59.06 Å, suggesting a mesoporous nature of the sample. Pore size distribution and surface area analysis of the EPS sample are presented in Table S17. The correlation coefficient of the BET analysis was near unity, confirming the reliability of the measurements. These results indicate that the EPS sample possesses a relatively low surface area with a predominantly mesoporous structure, which coincides with the SEM results and, therefore, may influence its adsorption and functional properties in biotechnological applications.

3.10. EPS backbone analysis

3.10.1. Determination of functional groups by Fourier transform infrared (FTIR) spectroscopy

The FTIR analysis was carried out to determine the EPS chemical structure, and the resulting spectrum is presented in Fig. 8D. The technique allows us to determine the main functional groups of F2LB exopolysaccharide. In the above spectrum, it is observed a broad band centered at 3285 cm^{-1} that is assigned as the stretching vibration of hydroxyl groups (ν –OH) from sugar residues [80]. Another peak at 2924 cm^{-1} corresponds to the stretching vibration of C—H bonds (ν–C–H) from the sugar ring. Other bands corresponding to C—H groups bond vibrations can be identified from peaks at 1413 cm^{-1} (δ–CH_2) and 1370 cm^{-1} (δ –CH), respectively. Stretching vibration of glycosidic bonds (–C–C, –C–H, –C–O, –OH) and pyranosic rings are exhibited from 1200 to 900 cm^{-1} (νas C–O–C, ring). From the peaks ranging from 950 and 750 cm^{-1}, stretching vibration of anomeric rings of exopolysaccharide was observed. FTIR spectra data in triplicates are presented in Fig. S12.

3.10.2. Analysis of glycosidic linkages by HSQC-NMR spectroscopy

The first analysis of the HSQC 2D-NMR spectra was primarily done in the anomeric region (4.0–6.0 ppm for ^1H spectra) (see Fig. 9). Nine different spectra were found (A1-I1, randomly assigned by the TopSpin software), which were then compared to the Carbohydrate Structure Database (CSDB) with a literature search for specific polysaccharides containing the main monosaccharides obtained after HPAEC-PAD

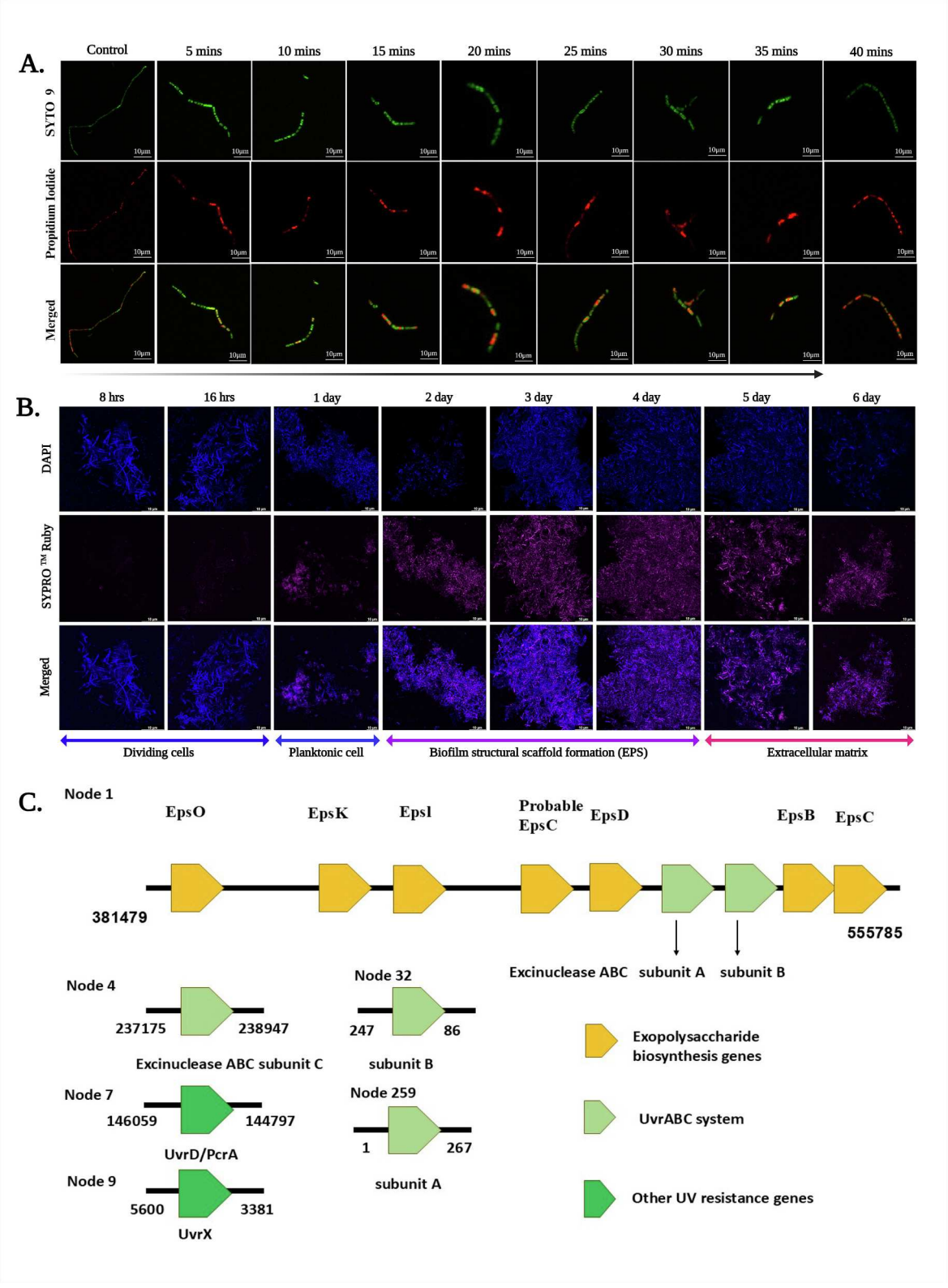

Fig. 6. A. Confocal micrograph demonstrating the morphological changes of *Bacillus licheniformis* F2LB under controlled UV exposure, **B.** Confocal microscopy analysis of the biofilm produced by *Bacillus licheniformis* F2LB over a 6-day period clearly illustrates the different stages of cell development during formation biofilm: division of cells (up to 16 h), planktonic cells (1 day), formation of the biofilm structural scaffold (2–4 days), and the development of the extracellular matrix (5–6 days), **C.** Exopolysaccharide biosynthesis genes and UV resistance related DNA repair genes from RAST whole genome assembly of *Bacillus licheniformis* F2LB. Polysaccharide pyruvyl transferase (EpsO), uncharacterized membrane protein (EpsK), polysaccharide pyruvyl transferase (EpsI),probable polysaccharide biosynthesis protein (EpsC), tyrosine-protein kinase (EpsD), manganese-dependent protein-tyrosine phosphatase (EpsB), tyrosine-protein kinase transmembrane modulator (EpsC) are depicted with yellow whereas, ultraviolet resistance genes like UvrABC system (Excinuclease ABC subunit A, B, C) are depicted in light green and ATP-dependent DNA helicase (UvrD/PcrA), putative UV-damage repair protein (UvrX) are presented in deep green. Observed contigs with their start and stop are mentioned.

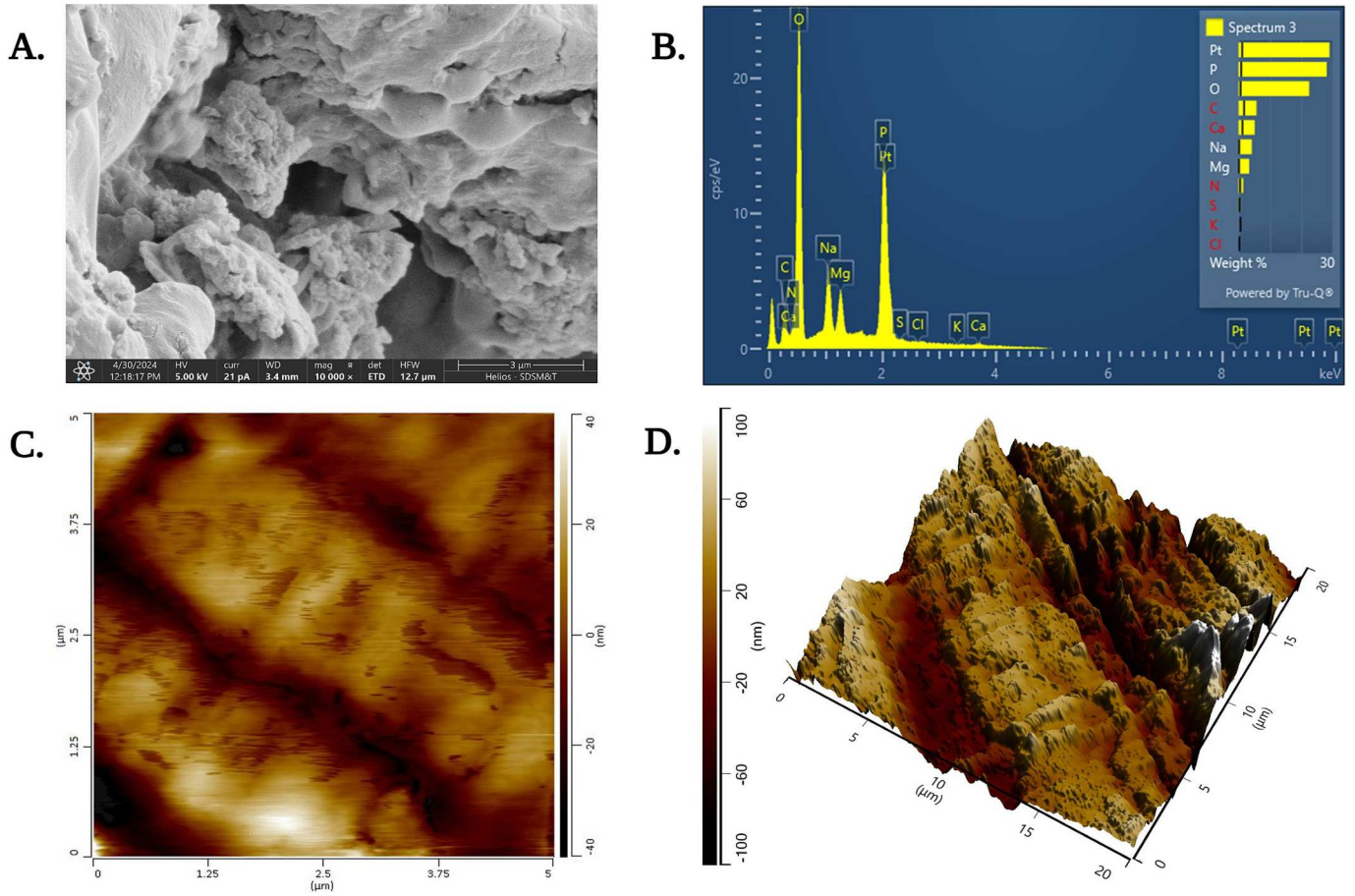

Fig. 7. Morphological analysis of EPS produced by *Bacillus licheniformis* F2LB by A. scanning electron microscopy and atomic force microscopy B. energy dispersive X-ray spectroscopy (EDS) C. 2D and D. 3D AFM image.

analysis (mannose, xylose, glucose, galactose, arabinose, fucose). A set of different glycosidic linkages was obtained (Table S18), but no spectra fit any xylose and arabinose anomeric carbons. This could be due to the limitations of the NMR technique since exopolysaccharides hydrolyzed by 2M TFA can be stably analyzed by HPAEC-PAD – at least the non-modified sugars [81]. The comparison of the anomeric carbons returned two possible backbones of polysaccharides ([→3)-β-Glcp-(1→] substituted and [→1)-α-Manp-(2→]). This is due to the comparison of observed linkages by the anomeric region spectra resulting from the probable linkages between the glucose from →3)-β-Glcp-(1→ and monosaccharides other than the mannose from →1)-α-Manp-(2→ (Table S18). Downshifted C6 spectra were observed, demonstrating a possible 6-substituted residue that the exopolysaccharides could have. However, an extensive analysis should be done to confirm the fine structure of the EPS. The sample was formed by two sets of polysaccharides, as corroborated by the HPSEC-RID chromatogram, which was divided into two main peaks: one between 330 kDa and 8 kDa (#1) and another below 5 kDa (#2). All the anomeric spectra were integrated, and the corresponding percentages are shown below the $^{1}H/^{13}C$ values in Table S18. Because the integrated percentage is higher for the glucose backbone than the mannose backbone, and with all other integrated areas summed in the glucose backbone, we inferred that the higher exopolysaccharide distribution seen in peak #1 after the HPSEC-RID analysis is the polysaccharide with the →3)-β-Glcp-(1→ substituted backbone (letter A and letter B as a →1 terminal linkage). And the smaller one is the one with the →1)-α-Manp-(2→ backbone (letter C and letter E as a →2 terminal linkage).

3.11. Elucidation of the functional properties of thermophilic EPS

3.11.1. In vitro antioxidant activity determination

In vitro antioxidant activity of F2LB EPS against H_2O_2, DPPH, Fe (II), and Fe^{2+} was demonstrated in Fig. 10A–D. H_2O_2 scavenging activity of EPS produced by F2LB was nearly 100 % and comparable to that of ascorbic acid across all concentrations (Fig. 10A). The statistical analysis by two-way ANOVA with Bonferroni's multiple comparisons test was carried out (Table S19) and the presence of statistical differences was observed between the 4 mg mL^{-1} concentration of the EPS in comparison with the rest of the concentrations analyzed ($p < 0.0001$), however between EPS and ascorbic acid there are no significant statistical differences. Even the lowest % RSA by the F2LB EPS was 98 ± 0.68.

It was found that % of DPPH radical scavenging gradually decreased with the increasing concentration of our studied EPS (Fig. 10B). At 1 mg mL^{-1} concentration, % of DPPH radical scavenging was highest (75.5 ± 0.19). In contrast, it was lowest in 5 mg mL^{-1} concentration (60.3 ± 8.74). However, almost 90 % of DPPH radical scavenging was observed in the case of ascorbic acid under all tested concentrations. The statistical analysis by two-way ANOVA with Bonferroni's multiple comparisons test was carried out on the DPPH antioxidant activity (Table S20). It was found that there is a statistical difference between all the concentrations of EPS and the concentrations of ascorbic acid ($p < 0.0001$); in addition, there are differences in the concentration of 5 mg mL^{-1} ($p < 0.0001$) of EPS for the other concentrations ($p < 0.0379$), the same is observed in the concentrations of ascorbic acid.

In terms of μM Fe (II) iron equivalents, our studied F2LB EPS outperformed commercial bacterial polysaccharide xanthan gum in all of the available concentrations (Fig. 10C). The μM Fe(II) iron equivalents

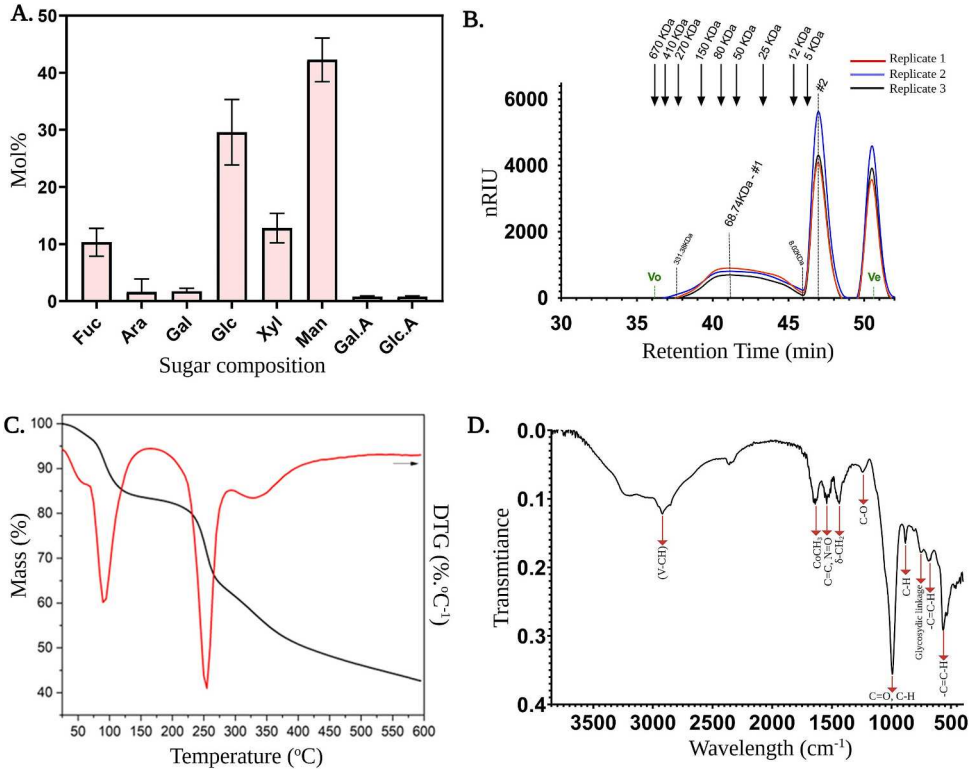

Fig. 8. A. HPLC analysis of the constituting monosaccharides of the EPS *Bacillus licheniformis* F2LB **B.** Molecular weight of F2LB EPS showing two diffraction **C.** Thermogravimetry of F2LB exopolysaccharide. Black line represents the mass loss in percentage (left scale); red line represents the derivative thermogravimetry (percentage/°C, right scale) **D.** FTIR spectrum showing the functional groups present of F2LB exopolysaccharide.

Table 2
Thermogravimetric analysis of the exopolysaccharide rom *Bacillus licheniformis* F2LB.

Sample	Temperature (°C)			Mass loss (%)	Char (%) (600 °C)
	T_{Onset}	T_{Peak}	T_{End}		
EPS F2LB	25	90	165	17.2	42
	166	255	293	21.3	
	294	328	435	13.8	

increased gradually with increasing concentration of the samples (maximum 143.9 ± 88.5 at 5 mg mL^{-1} concentration), while in case of commercial xanthan gum along with the increasing concentrations μM Fe(II) iron equivalents remains nearly similar. Statistical analysis by two-way ANOVA with Bonferroni multiple comparisons test was also performed on iron equivalents, where it was observed that there are significant statistical differences between the concentrations of xanthan gum and EPS ($p < 0.0001$), in addition to statistical differences between concentrations of the same group (Table S21).

It was observed that at 3 mg mL^{-1} concentration, Fe^{2+} iron chelation activity was highest (82.8 ± 1.26 %), whereas at 5 mg mL^{-1} concentration, it was lowest (71.64 ± 2.14 %). However more or less 100 % Fe^{2+} iron chelation activity was observed in case EDTA (Fig. 10D). Upon execution of statistical analysis by two-way ANOVA with Bonferroni multiple comparisons test it was found that there is significant statistical difference of the 5 mg mL^{-1} concentration, compared to 1 mg mL^{-1} ($p < 0.0464$), 2 mg mL^{-1} ($p < 0.0001$), 3 mg mL^{-1} ($p < 0.0001$) and 4 mg mL^{-1} ($p < 0.0001$) concentrations in F2LB EPS (Table S22).

3.11.2. Analysis of emulsification activity

In this study, emulsifying activities of our studied EPS were performed using edible oils like sesame, sunflower, canola, olive, corn, grape seed, vegetable, and rice oil, which are shown in Fig. 10E. It was observed that almost 90 % (89.89 ± 1.73) of emulsions was achieved in olive oil in 2 mg mL^{-1} concentration of EPS. However, the EPS produced by *B. licheniformis* F2LB can stabilize all other edible oils utilized in this experiment with at least 55 % emulsion in 1, 3, and 5 mg mL^{-1} concentrations. Upon execution of statistical analysis by two-way ANOVA with Bonferroni multiple comparisons test (Fig. S13 and Table S23), a significant statistical difference was observed in emulsifying activity index with olive oil ($p < 0.01$) between the application of 1 mg mL^{-1} and emulsifying activity index observed at concentrations of 2 and 5 mg mL^{-1}, respectively.

3.12. Water-holding and oil-holding capacity determination

The studied F2LB EPS showed 238.66 ± 3.05 % of water retention (WHC). However, in previous reports, the control xanthan gum showed 183.3 % [5], which is lower than our studied EPS. The OHC of our studied EPS was 384.66 ± 18.14 %. However, it was 111.0 % for xanthan gum, as found before in another study done by Banerjee et al. [5].

4. Discussion

The primary aim of this research is to analyze a novel EPS produced by thermophilic *Bacillus licheniformis* F2LB, which was isolated from Fumarole Bay located in the southwest of Deception Island in Antarctica. The rationale behind the experiments was that this thermophilic microorganism could produce novel exopolysaccharides for potential use in the pharmaceutical and food industry. Active volcanoes in Antarctica, such as the horseshoe-shaped stratovolcano in Deception Island, stand out amidst the predominantly frigid surroundings, fostering environmental conditions that favor versatile and highly varied microbial communities [82]. This uniqueness arises from the convergence of marine, geothermal, and polar environments, offering an exceptional spectrum of extreme environmental conditions due to

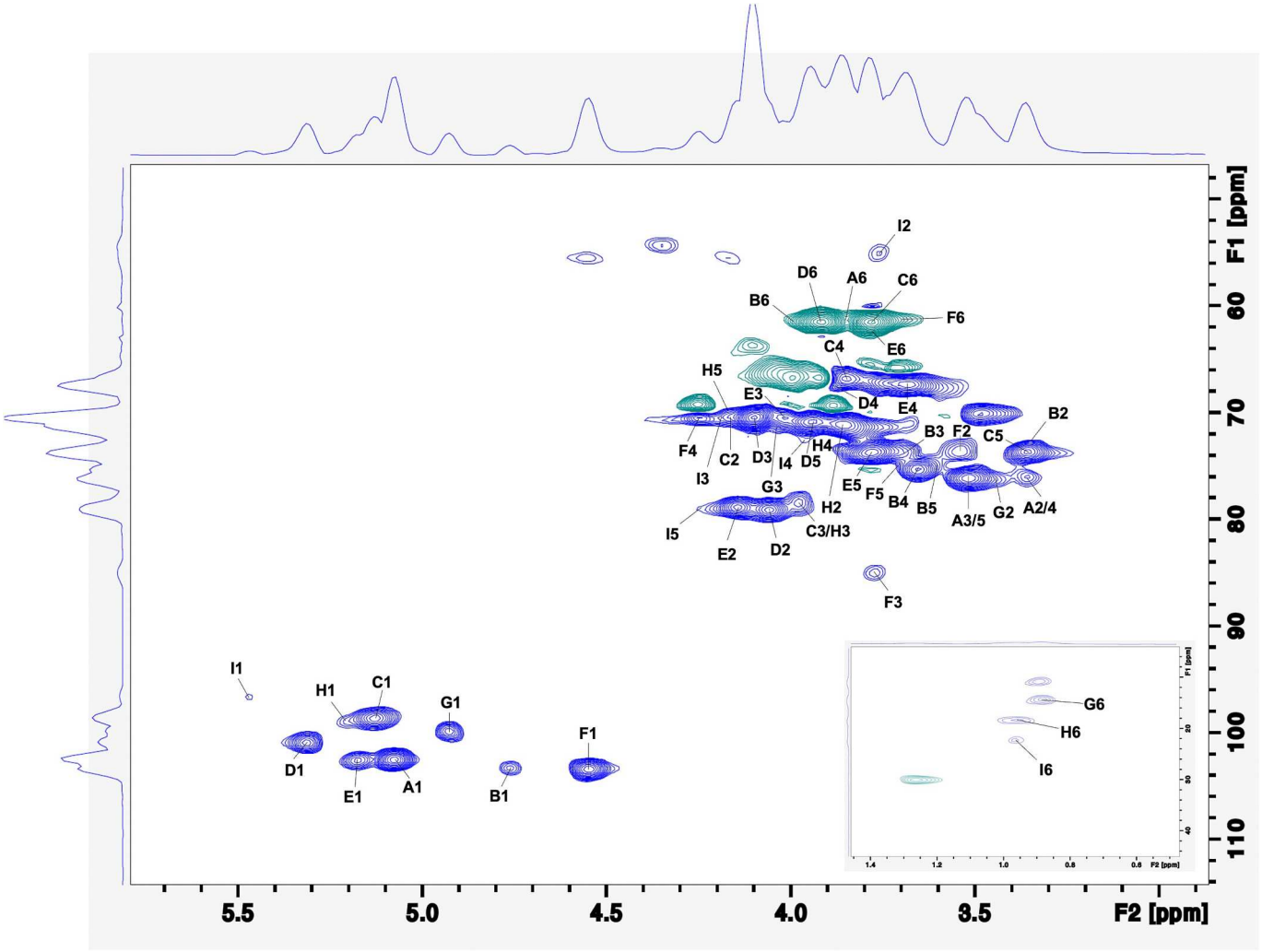

Fig. 9. A. HSQC-NMR spectrum of the EPS produced by *Bacillus licheniformis* F2LB.

highly versatile temperature, salinity, and geochemical gradients [83]. High salt content and slightly acidic nature of Fumarole Bay implies deep volcanic thermal water. It was assumed that approximately 10,000 years ago, the central part of the horseshoe-shaped stratovolcano collapsed, raising the Caldera Port Foster Bay during a magmatic eruption [84]. It was reported that most geothermal anomalies in Fumarole Bay originated due to the last eruption between 1967 and 1970 [85]. Considering the fact that the microbial communities residing in these geothermal fluids encounter a variety of extreme conditions, including temperature fluctuations, acidic pH levels, exposure to UV radiation, high salinity, and the enrichment of metals [82] in recent years, there has been a significant focus on investigating poly-extremophilic ecosystems to comprehend microbial biodiversity and utilize their biotechnological potential. Extremophiles, due to their ability to withstand harsh conditions, are recognized for producing several compounds to make them more resistant, which can contribute to the potential biotechnological applications [25,29–31]. Recently, very little research has been reported about the microbial life forms and their bioactive compounds' potential to thrive in the polyextreme environment of Antarctica, specifically Deception Island, which is the primary focus of our study [21,86–88].

In this regard, a strain designated F2LB was isolated, and preliminary analysis showed the presence of EPS production. Strain F2LB optimally grew at 55 °C, pH seven, and NaCl concentration 2 % (*w/v*). The 16S rRNA gene sequence of strain F2LB showed 100 % similarity to the type strain of *Bacillus licheniformis*. The 16S rRNA gene sequence similarity between F2LB and *B. licheniformis* was above the threshold (98.65 %) for species delineation [89], indicating they were similar species. In the phylogenomic tree (Fig. 2A), strain F2LB clade with *B. licheniformis*. The ANI value between F2LB and *B. licheniformis* was 99.5 %, which was above the threshold (95–96 %) for species delineation [90], indicating they were similar species. Deception Island is notable for its intense UV radiation and sharp temperature gradients (with fumaroles reaching 100 °C while nearby areas can be subzero) [21]. In 2018, Dzeha et al. reported a *B. licheniformis* strain BLC-01 (GeneBank ID KC660142) with the ability to cluster themselves, increasing their colony size upon UV radiation [91]. In this regard, our strain F2LB showed tolerance to 35 min (20.9 KJ/m^2) of gradual increase of UV-B exposure. The UVR complex genes were reported to repair DNA damage caused by exposure to UV radiation [92]. *B. licheniformis* F2LB encodes the uvrABCD genes, suggesting its mechanisms for mitigating UV-induced stress. *B. licheniformis* F2LB genome analysis showed the presence of heat shock proteins, cold shock proteins, and cellular chaperone machinery (cspA, htpX, htpG, hslO, dnaJ, dnaK, and grpE) capable of repairing cold and heat-induced protein damage [93,94]. In the genome of *B. licheniformis* F2LB, genes for proline and betaine biosynthesis were also observed. Proline and betaine are the osmolytes that accumulate in microbes in response to environmental stress [95]. *B. licheniformis* F2LB produced biofilm, and biofilm formation has already been reported as a successful strategy for microorganisms to survive in hostile environments [96]. The EPS produced by *B. licheniformis* F2LB showed a compact surface with a nonporous and rough structure. The roughness was mainly due to

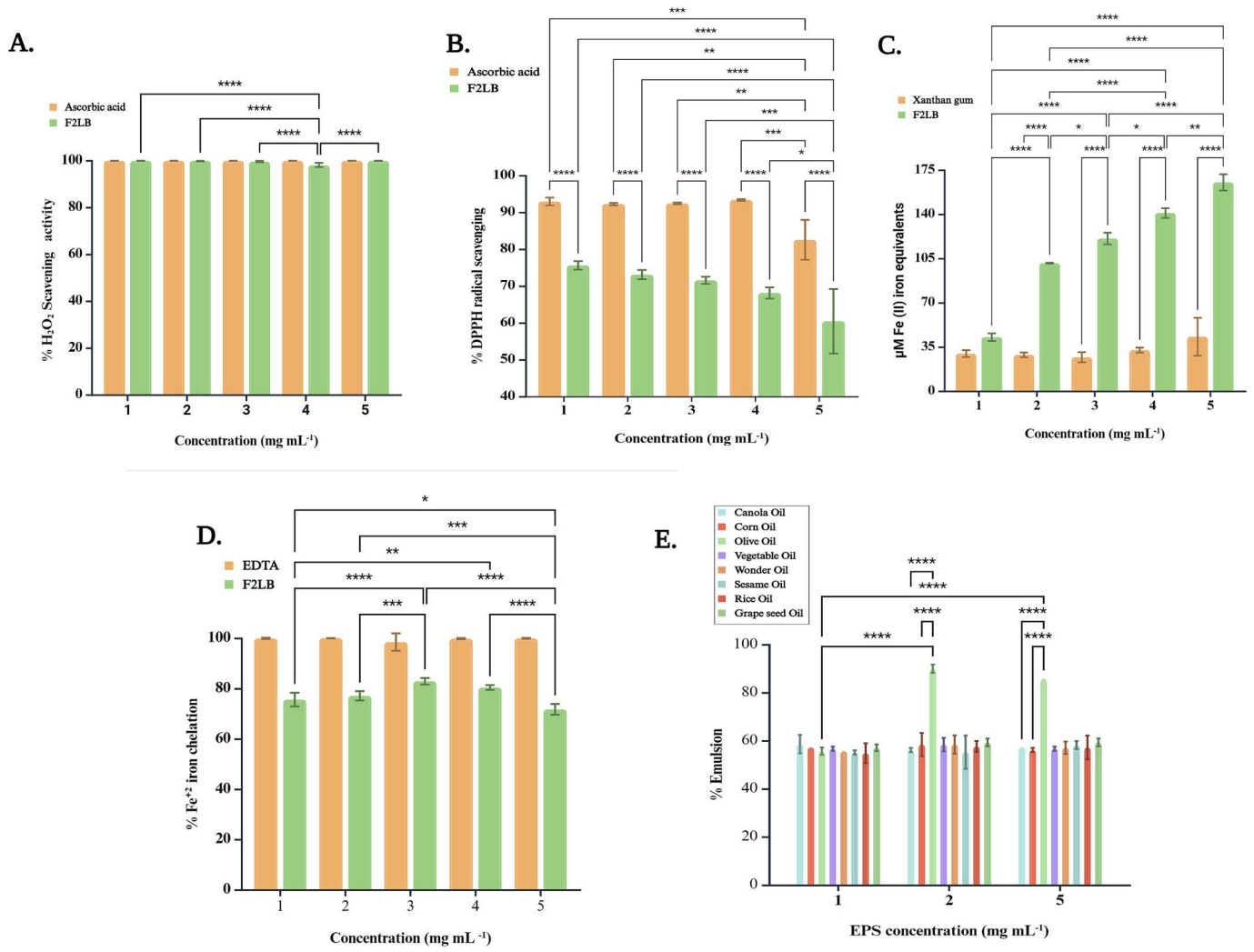

Fig. 10. In vitro antioxidant capability of the EPS produced by *Bacillus licheniformis* F2LB; where **A.** H_2O_2 radical scavenging activity **B.** DPPH radicle scavenging activity **C.** Fe (II) iron equivalents **D.** Fe^{2+} iron chelation activity and **E.** emulsifying activity of our studied EPS was performed using edible oils.

dispersed, undulated macromolecular lumps. Similar kinds of work have been reported in recent years from marine-origin bacteria with mannose and glucose majorly in their monosaccharide composition, similar to our study [76,77] [65,66]. The EDS micrograph revealed that *B. licheniformis* F2LB EPS was composed of carbon (41.88 %), oxygen (18.64 %), and phosphorus (14.98 %), and the presence of trace amounts of nitrogen (1.19 %) and sulfur (0.49 %) while in *B. haynesii* CamB6 the EPS was reported to be composed of carbon (52.52 %) and oxygen (47.48 %) and traces amount of (<0.5 %) of nitrogen, sulfur, and phosphorous elements [5]. The presence of diverse cations in the EDS micrograph, such as Ca, Mg, and Na, may be attributed to the metal-binding properties of EPS or its ion-exchange capabilities [97–101]. Nkoh et al. studied the electrokinetic mechanism of metal sorption on the EPS matrix and demonstrated that the binding of cations to the EPS matrix is driven by entropy changes during secretion [102]. The study further suggested that the sorption of cations occurs when the EPS carries a net negative charge, contributing to the neutralization of its overall charge. Buey et al. investigated the interaction of the EPS matrix with submerged clay surfaces and demonstrated a preferential trapping of Ca^{2+} cations within the EPS matrix [101]. This suggests the potential for cation precipitation within the matrix. Our study also revealed a cation chelation effect, strongly indicating its tendency to trap cations within the purified matrix. Bourven et al. investigated the mineral fractions in EPS derived from activated sludge using various extraction methods [103]. They observed that the extraction method significantly influenced the concentrations of Ca, Mg, Na, K, Al, Fe, Mn, P, Si, and S. Their study further reported that chelating agents, such as EDTA, notably reduced the levels of these cations. However, our current study did not employ any chelating agents during the extraction procedure. Bramhachari and Nagaraju reviewed EPS from marine environments and documented that EPS produced by marine bacteria exhibits a higher tendency for cation chelation [104]. This observation aligns with the marine origin of the isolate studied in our research. The composition of EPS macromolecules can vary significantly across different strains of *B. licheniformis*, reflecting the strain-specific biosynthetic pathways and environmental conditions influencing EPS production. In this study, the EPS produced by *B. licheniformis* F2LB consisted of mannose, glucose, xylose, fucose, arabinose, and galactose. Furthermore, substituents such as galacturonic acid and glucuronic acid were observed in *B. licheniformis* F2LB EPS. The diverse monosaccharide composition, including significant contributions from mannose, galactose, and glucose, is also critical in shaping the molecular interactions that underline its surface features [105,106]. Literature has shown that monosaccharides like mannose and glucose promote extensive hydrogen bonding, which can lead to the formation of denser, more cohesive matrices [107,108]. Singh et al. analyzed the monosaccharide composition of a *Bacillus* EPS (glucose, galactose, mannose, arabinose) with a molecular weight of 44,565 kDa. They highlighted the acidic sugars for

their crosslinking and structural roles, which ultimately affect roughness (191 nm) [109]. Acidic functional groups, including uronic acid-based phosphodiester linkages, mediate ionic and covalent interactions with surfaces, sometimes correlated with nanoscale features [110,111]. Studies examined the surface topology of EPS from *B. licheniformis* and *B. subtilis*, highlighting their porous surface nature. They reported that acidic monosaccharides (e.g., glucuronic acid and carboxyl/hydroxyl groups) are related to functionalization, leading to water retention and matrix structure [112,113]. Non-acidic monosaccharides reducing crosslinking density led to smooth surface features [110,112], as observed in our study. The presence of galactose and other minor sugar residues introduces branching and irregularities that contribute to the complex topography observed in the AFM images [114,115]. Furthermore, the molecular weight distribution significantly influences the EPS's physical properties [116,117]. Higher molecular weight fractions correlate with increased structural rigidity and enhanced adhesion capabilities, as these larger polymers can form extended network structures that resist deformation [118]. Conversely, lower molecular weight components may facilitate more flexible regions within the matrix, thereby contributing to the overall heterogeneity of the surface [15,119]. A study by Asgher et al. [120] demonstrated that the *B. licheniformis* MS3 strain consists of a heteropolymeric nature of its EPS, consisting solely of mannose (20.60 %), glucose (46.80 %), and fructose (32.58 %) subunits. Interestingly, the monosaccharide profile of EPS can also shift depending on the strain. For example, *B. licheniformis* T14 produces EPS primarily composed of fructose, fucose, and glucose, highlighting the variability in EPS structures across strains [121]. These differences underscore the influence of genetic and metabolic factors in determining the monosaccharide composition of EPS. In contrast, the EPS of *Lactobacillus paraplantarum* KM1 consists of only glucose, mannose, and galactose [122]. The AFM analysis of the EPS revealed an average surface roughness of 74.54 nm, indicative of a distinctly textured surface morphology. The structural complexity of the EPS observed from the AFM analysis is likely facilitated by the polysaccharide's heterogeneous monosaccharide composition and molecular weight variations, as evidenced by HPSEC results. Surface roughness is critical in enhancing the interaction between the EPS and biological entities, such as cells and biomolecules. Textured surfaces provide increased surface area and facilitate stronger binding interactions compared to smoother surfaces, thereby improving the functional efficacy of EPS in various applications. This phenomenon aligns with previous findings reported by Singh et al. [76], where the EPS from *B. licheniformis* RP-GC exhibited a higher roughness average of 191 nm, further underscoring the variability of roughness parameters across different microbial sources. It is important to recognize that the molecular structure and composition of the EPS strongly influence surface roughness and morphology. Our F2LB EPS was found to be predominantly mesoporous from BET analysis. Recently, *Planococcus rifietoensis* AP-5 from deep-sea sediments of the Northwest Pacific was also reported to produce mesoporous, large molecular weight, thermostable EPS consisting of majorly mannose and glucose, and demonstrated strong functional immunomodulatory potential [123]. Factors such as the arrangement of polysaccharide chains, the presence of specific functional groups, and the degree of branching in the polymer significantly contribute to these characteristics.

The highest optimized yield of the EPS produced by *B. licheniformis* F2LB was 0.992 g L^{-1} in yeast extract media at 55 °C, which is 0.43 g L^{-1} in preoptimized condition. Previously, *Bacillus licheniformis* strain T14 isolated from the shallow marine hydrothermal vent of Panarea Island, Italy, produced 0.366 g L^{-1} at 50 °C temperature under optimized conditions using media containing 5 % sucrose and 0.1 % yeast extract [124]. In 2015, Dogan et al. reported that *B. licheniformis B22* strain isolated from Pamukkale thermal region of Turkey produced a maximum EPS yield of 0.247 g L^{-1} when Cr (VI) used as a stressor in alginic acid-containing media at 50 °C [15]. *Bacillus licheniformis* MS3 strain was reported to produce 15.6 g L^{-1} EPS upon optimal usage of 7.5 g of carbon source as substrate, 0.55 g of nitrogen source (yeast extract), and an inoculum size of 3.5 mL, whereas in preoptimized condition it was 4.6 g L^{-1} [125].

Our studied EPS sample consisted of two distinct polysaccharide fractions, as confirmed by the HPSEC-RID chromatogram and analysis of glycosidic linkages by HSQC-NMR spectroscopy, which displayed two primary peaks: one ranging from 330 KDa to 8 KDa (Peak #1) and another below 5 KDa (Peak #2). Polar high molecular weight heterogenous polysaccharides can be considered as hydrocolloids. Their solubilization in water can produce a suspension-like aqueous solution with an increment in the rheology of the system. When dried, a film is formed with different structures. This is due to the physical interaction of the polysaccharides' chains [126]. As mentioned before, our study identified a high molecular weight heterogeneous (different sugar composition) polysaccharide (330KDa) considered a hydrocolloid. When dried, the film was formed with varying microstructures, as explained before. Regarding exopolysaccharide #1, a comparative analysis between the anomeric carbon spectra and the CSBD database and literature indicated the same backbone was present in different microorganisms found in pulmonary diseases (*Moraxella catarrhalis* and *Streptococcus pneumoniae*) [127,128]. The ramification of the glucose backbone starts with a galactose being directly linked to the glucose backbone (letter F as →t-β-Gal*p*), with the →1)-β-Glc*p*-(3→1)-β-Glc*p*-(3→4)-β-Gal*p* structure found in the indicated pulmonary microorganisms. The glucose ramifications follow mannose residues linked to the fourth glucose carbon (letter D as →4)-α-Man*p*-(1→) that can be further connected with a terminal galactose. This type of linkage is found in some pathogenic *Salmonella* spp. [129,130]. The other polysaccharide terminal was decorated by →1)-α-L-Fuc*p*-(3→ glycoside linkages (letter G and letter H as terminal). This type of linkage was found in glycolipids from *Mycobacterium kansasii*, a mycobacterium that can cause lung colonization or infection, being an opportunistic pathogen [131]. This double fucose is finally attached to an L-Fuc*p*N terminal linkage by 1,3-α to the fucose, a type of glycoside bound found in the lipopolysaccharide of *Pseudomonas aeruginosa* [132,133]. The second polysaccharide is mainly formed by a →1)-α-Man*p*-(2→ backbone, and this type of polysaccharide is found in several *Escherichia coli* subtypes [67]. Two exopolysaccharides produced by a Chilean hot spring-origin *Staphylococcus* sp. were described as having the same backbone structure. BSP3 and *Pseudomonas alcaligenes* Med1, demonstrating that the sugar mannose in an α-1,2 glycosidic linkage might be crucial for stabilizing the produced polysaccharide in high saline concentration and temperature [1,134–136]. Despite some other experiments that need to be done to get the complete structures of *B. licheniformis* F2LB exopolysaccharides, our approach could identify a putative glucogalactomannan-backbone polysaccharide produced by this thermophilic microorganism.

B. licheniformis F2LB EPS demonstrated higher thermal stability (T_{peak} of 255 °C) than other EPS isolated from bacterial strains from the same genus, demonstrating the ability of the bacterium to make an external microenvironment more prone to survive. For example, the thermostable EPS WSF-1, which was composed of fructose and glucose, has a T_{peak} of 219 °C [137]. Additionally, the reported T_{peak} of the EPS from *Bacillus licheniformis* PASS26 is around 200 °C [75]. The primary sugars were mannose and galacturic acid, which were followed by fructose, glucose, and mannose. In contrast, the thermal stability of hot spring-origin *Staphylococcus* sp. BSP3 EPS, mainly composed of mannose (72 %), glucose (24 %), and galactose (4 %), was reported to be higher (T_{peak} 287 °C) than found in the present work [1]. Thermal stability is one of the vital factors to be considered when incorporating bacterial EPSs in commercial applications. Thermally stable EPSs are highly desirable for food applications because they maintain their structural integrity and functional properties under high-temperature processing conditions commonly used in the food industry [138]. EPS from *Lactobacillus plantarum* HM47 reported a maximum degradation temperature (T_d) of 273.6 °C or commercial application as a food additive [139]. A gastroprotective and antioxidant EPS produced by *Streptococcus*

thermophilus CRL1190 with a T_d of 295.4 °C also reported to be used for the food industry with microporous, rough surface and functionality in both aqueous and oil systems [140]. Thermally stable polysaccharides induce heat resistance in food processing, improve shelf-stability, enhance food texture, sustain bioactive potential, and are compatible with various food matrices [141].

Genome analysis showed that the *B. licheniformis* F2LB genome was 98.8 % complete with 0.4 % contamination, indicating a good-quality genome [39]. *B. licheniformis* F2LB encodes genes for glycolysis, citric acid cycle, and pentose phosphate pathway. *B. licheniformis* F2LB encode genes for dissimilatory nitrate reduction (through nitrate reductase narGHI and nitrite reductase nirBD) and assimilatory sulfate reduction (through sat, cysC, cysH, and cysJI) similar to EPS producing *B. paralicheniformis* CamBx3 isolated from hot spring [142]. The biosynthesis of EPSs involves regulation, chain-length determination, repeat-unit assembly, polymerization, and export [143]. The initial synthesis consists of sugar uptake through the phosphoenolpyruvate-phosphotransferase system (PEP-PTS) and permease [144,145]. Genome analysis of *B. licheniformis* F2LB showed the presence of PEP-PTS and permease for the uptake of glucose, galactose, fructose, sucrose, maltose, mannose, xylose, arabinose, lactose, and cellobiose. Further, the sugars were converted into nucleotide sugars via different pathways. *B. licheniformis* F2LB encodes genes for converting glucose to UDP-glucose (*glk*, *pgm*, *galU*) and UDP-galactose (galE). Similarly, *B. licheniformis* F2LB contains genes responsible for converting trehalose (treC), cellobiose (bglA), and maltose (malZ) into glucose-6-phosphate. It also encodes genes for converting glucose-6-phosphate into UDP-glucose (glk, pgm and galU) and UDP-galactose (galE). In addition, cellobiose, trehalose, maltose, and sucrose may also convert to fructose 6-phosphate (glmS, glmM, glm, and glmU) to UDP-*N*-acetylglucosamine. *B. licheniformis* F2LB encodes the genes for converting fructose, mannose, xylose, and arabinose to fructose 6-phosphate and subsequently to UDP-*N*-acetylglucosamine. *B. licheniformis* F2LB showed the presence of epsA, epsB, epsD, epsE, epsF, epsG, epsM and epsN genes for EPS chain length determination, biosynthesis of repeating sugar units and EPS polymerization and export [146]. The detailed EPS production pathway is depicted in (Fig. 3).

The functional activity of the isolated EPS was also studied to demonstrate its capability to be used as a natural additive in the future food industry. Antioxidants can play a crucial role in preventing oxidation processes caused by reactive oxygen species (ROS), making them beneficial for use in food additives or stabilizers for active ingredients in the pharmaceutical industries. The EPS was reported to have antioxidant activity [147,148]. DPPH is an important reagent for evaluating free radical scavenging since it reduces the DPPH radical. Antioxidants neutralize the DPPH radical by donating electrons or hydrogen atoms, resulting in a color change. The magnitude of this color change (as assessed by a decrease in absorbance) is related to the amount of antioxidants in the sample [69]. H_2O_2 scavenging activity was also used to determine antioxidant capacity. Hydrogen peroxide scavenging activity refers to the ability of a substance to neutralize H_2O_2, a reactive oxygen species that can cause oxidative stress and damage to cells [68]. In addition, the FRAP assay was also carried out to measure the antioxidant capacity of a substance by its ability to reduce ferric ions (Fe^{3+}) to ferrous ions (Fe^{2+}) [70]. *B. licheniformis* F2LB EPS showed 100 % hydrogen peroxide scavenging activity and 75.5 % DPPH radical scavenging activity, while the EPS produced by *Bacillus subtilis* LR-1 showed 93.23 % hydroxyl radicals and 77.65 % DPPH activity [149]. Recently, Alharbi et al. reported a sulphated EPS produced by *B. licheniformis* LHG166 isolated from the western shores of the Red Sea, Saudi Arabia, which also showed a similar trend of DPPH activity (highest percentage of scavenging of 79.9 % at 1 mg mL^{-1} concentration) which has 17.40 % sulfate groups and 48.11 % uronic acid in its monosaccharide composition [150]. In terms of μM Fe(II) iron equivalents, *B. licheniformis* F2LB EPS outperformed commercial bacterial polysaccharide xanthan gum in all of the available concentrations. The melting point of this EPS at 90 °C is much lower than that of xanthan gum with 153.4 °C. Previously, the EPS produced by *Lactobacillus kefiranofaciens* showed similar behavior where a lower melting point has been related to better functional activity [151]. Additionally, in several instances [152,153], compositionally diverse bacterial EPSs outperformed the functional activities of commercial xanthan gum, which is mainly composed of Glucose, Mannose, and Glucuronic acid [154]. Some monosaccharides naturally modified (such as fucosamine) could exert radical scavenging potential. Moreover, polysaccharides can also chelate iron, thus showing the antioxidant effects observed in our experiments. The antioxidant properties of the EPS can also be related to other chemical compounds chemically bound to polysaccharides, but they were not determined in the present study. The ability of polysaccharides to neutralize free radicals and protect against oxidative damage is due to their molecular structure. For example, the presence of glucose and galactose in the structure of certain polysaccharides is associated with a greater capacity to eliminate free radicals, owing to the reducing properties of these monosaccharides [155]. Additionally, functional groups such as hydroxyl and carboxyl groups can enhance antioxidant activity by facilitating electron donation to neutralize reactive oxygen species [156]. Studies have shown that the molecular weight of polysaccharides can influence antioxidant activity, with lower molecular weight polysaccharides exhibiting higher antioxidant activity, possibly due to their better solubility and ease of interaction with free radicals [157]. However, other studies suggest that greater structural complexity, associated with higher molecular weight, can contribute to more robust antioxidant activity, indicating that the relationship between molecular weight and antioxidant activity may vary depending on the source and specific structure of the polysaccharide [158]. The structure of the polysaccharide is affected by the configuration and position of glycosidic bonds, which alter its biological activity. β-(1→3) and β-(1→6) linkages in β-glucans have been reported to be associated with significant antioxidant properties, possibly due to their ability to form helical structures that facilitate interactions with free radicals [156]. The presence of α-(1→4) linkages has also been linked to enhanced antioxidant activity in certain polysaccharides [159]. In our study, the emulsifying activity of *B. licheniformis* F2LB EPS was evaluated with various oils, including sesame, sunflower, canola, olive, corn, grape seed, vegetable, and rice oil. Among all the edible oils tested, *B. licheniformis* F2LB EPS achieved ~90 % emulsification in olive oil (2 mg mL^{-1}). Bacterial EPSs are used as commercial additives due to their favorable physicochemical properties, superior surface activity, biodegradability, high specificity, low toxicity, and effectiveness in extreme conditions [7,160]. WHC is one functional property of EPS highly influenced by molecular weight and chemical composition [161]. Previously, one studied EPS from hot-spring-origin *B. haynesii* CamB6 showed ~102 % WHC. However, *B. licheniformis* F2LB EPS showed 238.66 ± 3.05 % of water retention, much higher than even the control xanthan gum, previously reported to be 183.3 % [5]. The OHC of *B. licheniformis* F2LB EPS was 384.66 ± 18.14 %. It was 111.0 % for xanthan gum, as found before in one study done by Banerjee et al., [5]. The OHC is an important property of the EPS that helps us understand the permeable structure of the polymer chain of EPS. OHC is one of the important characteristics of polysaccharides, indicating better adsorption of organic compounds or oils to the surface of substrates. Along with this, the porosity and the affinity of the biopolymer with the oil also contribute to the functional activity of the EPS. Hence, EPS with high OHC is useful as an additive in different food industries, such as sausage preparation [162]. *B. licheniformis* MS3 strain was reported to have 105.3 % WHC and 86.3 % OHC. This strain was also reported to have 61.8 and 64.8 % emulsification in Mustard and cottonseed oil [15]. Due to its good water-holding and oil-holding capacity, the EPS produced by *B. licheniformis* F2LB holds great potential as a valuable additive for future applications in the food industry.

Overall, the EPS produced by the thermophilic *B. licheniformis* F2LB exhibits antioxidants, emulsifying, and water/oil-holding capacities,

surpassing standard ascorbic acid and commercial xanthan gum in key functional properties. Its high thermal stability and unique monosaccharide composition make it a promising natural additive for food applications. While this study provides detailed structural and functional insights, future research should optimize production, assess its performance in real food systems, and explore its biodegradability and safety. These findings highlight the potential of thermophilic bacterial EPSs as sustainable bio-based ingredients for the food industry. However, other experiments must be done to guarantee the security of the EPS.

5. Conclusion

In the present study, a thermophilic *B. licheniformis* F2LB was isolated from Fumarole Bay in Deception Island, Antarctica. Analysis of the whole genome of the isolated bacterial strain demonstrated gene cluster for EPS biosynthesis, UV resistance, heat tolerance, and other significant metabolic potential. Extracted F2LB EPS was found to be composed of mainly mannose, glucose, xylose, fucose, arabinose, and galactose, along with the presence of galacturonic acid and glucuronic acid. Two sets of fractions, one from high to medium distribution and another with low molecular weight, were observed. This confirms the structural complexity of exopolysaccharides produced, which is probably responsible for high-temperature adaptation. The EPS exhibited potent antioxidant activity, including ~100 % $OH^{\bullet}$ scavenging, ~75 % DPPH radical scavenging, and a maximum Fe(II) reducing power of 143.9 ± 88.5 μM $FeSO_4$ equivalents, outperforming commercial xanthan gum at all tested concentrations. Additionally, Fe^{2+} chelation activity was highest at 82.8 ± 1.26 % at 3 mg mL^{-1} concentration, with significant statistical differences observed between concentrations ($p < 0.0001$). The emulsification activity reached ~90 % in olive oil while stabilizing all other tested edible oils at a minimum of 55 % emulsification. It showed thermal stability up to 255 °C. These results confirm our hypothesis of its significant potential as a natural, multifunctional food additive. However, other experiments must be done to indicate the fine polysaccharide structural features.

This study represents the first report of an EPS-producing bacterium from an Antarctic fumarolic environment. Furthermore, it provides a detailed structural characterization of the EPS and its functional properties, including its antioxidant and emulsification potential, which are relevant for biotechnological applications. Integrating genomic and functional analyses enhances our understanding of the adaptive strategies of extremophiles in extreme habitats. However, large-scale production and purification of the EPS remain challenging, requiring further optimization for industrial applications. Additionally, while in vitro evaluations confirm its functional potential, its real-world application in food systems and its long-term stability require further study. This research contributes to global sustainability by addressing key United Nations Sustainable Development Goals (SDGs). It supports SDG 2 Zero Hunger by offering a natural and sustainable food additive, promotes SDG 9 Industry, Innovation, and Infrastructure through bio-based technological advancements, encourages Responsible Consumption and Production by fostering environmentally friendly alternatives to synthetic additives, and aids in the conservation of Antarctic microbial biodiversity, contributing to Life Below Water (SDG 14). These findings highlight the importance of extremophiles in sustainable scientific and industrial developments.

CRediT authorship contribution statement

Aparna Banerjee: Writing – review & editing, Supervision, Resources, Project administration, Methodology, Investigation, Funding acquisition, Formal analysis, Data curation, Conceptualization. **João Paulo Fabi:** Writing – review & editing, Writing – original draft, Software, Resources, Methodology, Investigation, Formal analysis, Data curation. **Catherine Ormeño:** Investigation, Formal analysis, Data curation. **Srijan Banerjee:** Writing – original draft, Software, Data curation. **Nicolás Flores-Castañón:** Formal analysis. **Francisca Valenzuela:** Writing – review & editing, Software, Data curation. **Shrabana Sarkar:** Writing – original draft, Software, Data curation. **Alexander Galán:** Writing – review & editing, Formal analysis, Data curation. **Dipayan Samanta:** Writing – review & editing, Formal analysis. **Priya Saxena:** Writing – review & editing, Formal analysis. **Rajesh K. Sani:** Writing – review & editing, Resources. **Manik Prabhu Narsing Rao:** Writing – review & editing, Software, Formal analysis. **Gustavo Cabrera-Barjas:** Writing – review & editing, Writing – original draft, Investigation, Formal analysis.

Declaration of competing interest

The authors declare that they have no known competing financial interests or personal relationships that could have appeared to influence the work reported in this paper.

Acknowledgement

AB, CO, AG, RS, and GC-B acknowledge the support of the project INACH RT_24-21. AB, JPF, SS, AG, RS, and GC-B acknowledge the project FOVI220149 by ANID, Govt. of Chile. AB, JPF, SB, FV, and GC-B are thankful to Fondecyt Regular 1231917, ANID of Govt. of Chile. AB and AG acknowledge INACH and Gabriel de Castilla base, Spain, for all the logistic support and sampling during the Antarctica expedition in 2022 and 2023. JPF acknowledges the São Paulo Research Foundation (FAPESP) for partially funding the research (2013/07914-8 and 2022/12834-2). We are thankful to FONDEQUIP-ANID EQM200122 for the confocal microscopy, acknowledge Biorender for arrangement of the figures, and Cynthia Meza, Felipe Moraga, Isabel Vidal Beltrán, and Hanuxa Celedón González for their support during the experiments. AB acknowledges Alexis Castillo Bruna for his support during the expedition. This research used a nanoIR3 equipment which was funded by the National Science Foundation MRI Award # 2216292.

Appendix A. Supplementary data

Supplementary data to this article can be found online at https://doi.org/10.1016/j.ijbiomac.2025.146114.

Data availability

All the data are provided within supplementary materials.

References

[1] S. Banerjee, G. Cabrera-Barjas, J. Tapia, J.P. Fabi, C. Delattre, A. Banerjee, Characterization of Chilean hot spring-origin *Staphylococcus* sp. BSP3 produced exopolysaccharide as biological additive, Nat. Prod. Bioprospect. 14 (1) (2024) 15, https://doi.org/10.1007/s13659-024-00436-0.

[2] E.A. Eloe-Fadrosh, D. Paez-Espino, J. Jarett, P.F. Dunfield, B.P. Hedlund, A. E. Dekas, S.E. Grasby, A.L. Brady, H. Dong, B.R. Briggs, W.-J. Li, D. Goudeau, R. Malmstrom, A. Pati, J. Pett-Ridge, E.M. Rubin, T. Woyke, N.C. Kyrpides, N. N. Ivanova, Global metagenomic survey reveals a new bacterial candidate phylum in geothermal springs, Nat. Commun. 7 (1) (2016) 10476, https://doi.org/10.1038/ncomms10476.

[3] Y.L. Qi, Y.T. Chen, Y.G. Xie, Y.X. Li, Y.Z. Rao, M.M. Li, Q.J. Xie, X.R. Cao, L. Chen, Y.N. Qu, Z.X. Yuan, Z.C. Xiao, L. Lu, J.Y. Jiao, W.S. Shu, W.J. Li, B.P. Hedlund, Z. S. Hua, Analysis of nearly 3000 archaeal genomes from terrestrial geothermal springs sheds light on interconnected biogeochemical processes, Nat. Commun. 15 (1) (2024) 4066, https://doi.org/10.1038/s41467-024-48498-5.

[4] A. Chien, D.B. Edgar, J.M. Trela, Deoxyribonucleic acid polymerase from the extreme thermophile *Thermus aquaticus*, J. Bacteriol. 127 (3) (1976) 1550–1557, https://doi.org/10.1128/jb.127.3.1550-1557.1976.

[5] A. Banerjee, S.J. Mohammed Breig, A. Gómez, I. Sánchez-Arévalo, P. González-Faune, S. Sarkar, R. Bandopadhyay, S. Vuree, J. Cornejo, J. Tapia, G. Bravo, G. Cabrera-Barjas, Optimization and characterization of a novel exopolysaccharide from *Bacillus haynesii* CamB6 for food applications, Biomolecules 12 (6) (2022) 834, https://doi.org/10.3390/biom12060834.

[6] Y. Risjani, N. Mutmainnah, P. Manurung, S.N. Wulan, Yunianta, Exopolysaccharide from *Porphyridium cruentum* (purpureum) is not toxic and

stimulates immune response against Vibriosis: the assessment using zebrafish and white shrimp *Litopenaeus vannamei*, Mar. Drugs 19 (3) (2021) 133, https://doi.org/10.3390/md19030133.
[7] Y.M.M. Mohammed, M.M.G. Saad, S.A.M. Abdelgaleil, Production, characterization and bio-emulsifying application of exopolysaccharides from *Rhodotorula mucilaginosa* YMM19, 3 Biotech. 11 (7) (2021) 349, https://doi.org/10.1007/s13205-021-02898-2.
[8] M. Faustino, M. Veiga, P. Sousa, E.M. Costa, S. Silva, M. Pintado, Agro-food byproducts as a new source of natural food additives, Molecules 24 (6) (2019) 1056, https://doi.org/10.3390/molecules24061056.
[9] J. Wang, D.R. Salem, R.K. Sani, Extremophilic exopolysaccharides: a review and new perspectives on engineering strategies and applications, Carbohydr. Polym. 205 (2019) 8–26, https://doi.org/10.1016/j.carbpol.2018.10.011.
[10] K. Solymosi, N. Latruffe, A. Morant-Manceau, B. Schoefs, 1 - Food colour additives of natural origin, in: Michael J. Scotter (Ed.), Woodhead Publishing Series in Food Science, Technology and Nutrition, Colour Additives for Foods and Beverages, Woodhead Publishing, 2015, pp. 3–34, https://doi.org/10.1016/B978-1-78242-011-8.00001-5.
[11] S. Tiwari, D. Kavitake, P.B. Devi, P.H. Shetty, Bacterial exopolysaccharides for improvement of technological, functional and rheological properties of yoghurt, Int. J. Biol. Macromol. 83 (2021) 1585–1595, https://doi.org/10.1016/j.ijbiomac.2021.05.140.
[12] S. Zalma, W. El-Sharoud, Diverse thermophilic Bacillus species with multiple biotechnological activities are associated within the Egyptian soil and compost simples, Sci. Prog. 104 (4) (2021), https://doi.org/10.1177/00368504211055277.
[13] Syamsuardi Arzita, A. Agustien, Y. Rilda, The diversity of the alkaline protease producers, thermophilic obligate *Bacillus* spp., from Sungai Tutung Hot Spring, Kerinci, Jambi, Indonesia, J. Pure Appl. Microbiol. 11 (4) (2017) 1789–1797, https://doi.org/10.22207/JPAM.11.4.18.
[14] Z. Xu, G. Chen, L. Xue, H. Zhang, J. Wang, H. Xiang, J. Li, K. Zheng, Isolation, structural characterizations and bioactivities of exopolysaccharides produced by Bacillus licheniformis, Int. J. Biol. Macromol. 141 (2019) 298–306, https://doi.org/10.1016/j.ijbiomac.2019.08.217.
[15] M. Asgher, Y. Urooj, S.A. Qamar, N. Khalid, Improved exopolysaccharide production from Bacillus licheniformis MS3: optimization and structural/functional characterization, Int. J. Biol. Macromol. 151 (2020) 984–992, https://doi.org/10.1016/j.ijbiomac.2019.11.094.
[16] A. Vinothkanna, G. Sathiyanarayanan, A.K. Rai, K. Mathivanan, K. Saravanan, K. Sudharsan, P. Kalimuthu, Y. Ma, S. Sekar, Exopolysaccharide produced by probiotic Bacillus albus DM-15 isolated from Ayurvedic fermented Dasamoolarishta: characterization, antioxidant, and anticancer activities, Front. Microbiol. 13 (2022) 832109, https://doi.org/10.3389/fmicb.2022.832109.
[17] R. Orellana, C. Macaya, G. Bravo, F. Dorochesi, A. Cumsille, R. Valencia, C. Rojas, M. Seeger, Living at the Frontiers of life: extremophiles in Chile and their potential for bioremediation, Front. Microbiol. 9 (2018), https://doi.org/10.3389/fmicb.2018.02309.
[18] S. Cirés, M.C. Casero, A. Quesada, Toxicity at the edge of life: a review on cyanobacterial toxins from extreme environments, Mar. Drugs 15 (7) (2017) 233, https://doi.org/10.3390/md15070233.
[19] P.R. Kyle, J.W. Cole, Structural control of volcanism in the McMurdo volcanic group, Antarctica, Bull. Volcanol. 38 (1974) 16–25, https://doi.org/10.1007/BF02597798.
[20] C.W. Herbold, I.R. McDonald, I.C. Cary, Microbial ecology of geothermal habitats in Antarctica, in: D. Cowan (Ed.), Antarctic Terrestrial Microbiology, Springer, Berlin, Heidelberg, 2014, pp. 181–215, https://doi.org/10.1007/978-3-642-45213-0_10.
[21] A.G. Bendia, G.G. Araujo, A.A. Pulschen, B. Contro, R.T.D. Duarte, F. Rodrigues, D. Galante, V.H. Pellizari, Surviving in hot and cold: psychrophiles and thermophiles from Deception Island volcano, Antarctica, Extremophiles 22 (6) (2018) 917–929, https://doi.org/10.1007/s00792-018-1048-1.
[22] J.L. Smellie, J. López-Martínez, R.K. Headland, F. Hernández-Cifuentes, A. Maestro, I.L. Millar, J. Rey, E. Serrano, L. Somoza, J.W. Thomson, Geology and Geomorphology of Deception Island, British Antarctic Survey, Cambridge, 2002, p. 77.
[23] M. Lezcano, M. Moreno-Paz, D. Carrizo, O. Prieto-Ballesteros, M. Fernández-Martínez, L. Sánchez-García, Y. Blanco, F. Puente-Sánchez, G. de Diego-Castilla, M. García-Villadangos, A.G. Fairén, V. Parro, Biomarker profiling of microbial mats in the geothermal band of Cerro Caliente, Deception Island (Antarctica): life at the edge of heat and cold, Astrobiology 19 (12) (2019) 1490–1504, https://doi.org/10.1089/ast.2018.2004.
[24] A.T. Caselli, M. dos Santos Afonso, M.R. Agusto, Gases fumarólicos de la Isla Decepción (Shetland del Sur, Antártida): variaciones químicas y depósitos vinculados a la crisis sísmica de 1999, Rev. Asoc. Geol. Argent. 59 (2) (2004) 291–302.
[25] P.A. Muñoz, P.A. Flores, F.A. Boehmwald, J.M. Blamey, Thermophilic bacteria present in a sample from Fumarole Bay, Deception Island, Antarct. Sci. 23 (6) (2011) 549–555, https://doi.org/10.1017/S0954102011000393.
[26] A. Muñoz-Martín, M. Catalán, J. Martín-Dávila, A. Carbó, Upper crustal structure of Deception Island area (Bransfield Strait, Antarctica) from gravity and magnetic modelling, Antarct. Sci. 17 (2005) 213–224, https://doi.org/10.1017/S0954102005002622.
[27] J. Vicente, M. de Celis, A. Alonso, D. Marquina, A. Santos, Microbial communities present in hydrothermal sediments from Deception Island, Antarctica, Microorganisms 9 (8) (2021) 1631, https://doi.org/10.3390/microorganisms9081631.
[28] O. Carrión, D. Miñana-Galbis, M.J. Montes, E. Mercadé, Pseudomonas deceptionensis sp. nov., a psychrotolerant bacterium from the Antarctic, Int. J. Syst. Evol. Microbiol. 61 (10) (2011) 2401–2405, https://doi.org/10.1099/ijs.0.024919-0.
[29] M.A. Cabrera, J.M. Blamey, Cloning, overexpression, and characterization of a thermostable nitrilase from an Antarctic *Pyrococcus* sp, Extremophiles 21 (5) (2017) 861–869, https://doi.org/10.1007/s00792-017-0948-9.
[30] D.N. Correa-Llantén, M.J. Amenábar, P.A. Muñoz, M.T. Monsalves, M.E. Castro, J. M. Blamey, *Alicyclobacillus* sp. strain CC2, a thermo-acidophilic bacterium isolated from Deception Island (Antarctica) containing a thermostable superoxide dismutase enzyme, Adv. Polar Sci. 25 (2) (2014) 92–96, https://doi.org/10.13679/j.advps.2014.2.00092.
[31] P.A. Muñoz, D.N. Correa-Llantén, J.M. Blamey, Production, purification and partial characterization of four lipases from a thermophile isolated from Deception Island, Lipids 48 (5) (2013) 527–533, https://doi.org/10.1007/s11745-013-3771-9.
[32] E.L. Atlas, S.W. Hager, L.I. Gordon, P.K. Park, A Practical Manual for Use of the Technicon (Trade Name) Autoanalyzer (Trade Name) in Seawater Nutrient Analyses; Revised, Defense Technical Information Center, Oregon State University, Department of Oceanography. Technical report, 1971.
[33] J.D.H. Strickland, T.R. Parsons, in: The Alger (Ed.), A Practical Handbook of Seawater Analysis, Bulletin, Fisheries Research Board of Canada, Ottawa, 1972.
[34] S.E. Bunn, N.R. Loneragan, M.A. Kempste, Effects of acid washing on stable isotope ratios of C and N in penaeid shrimp and seagrass: implications for food-web studies using multiple stable isotopes, Limnol. Oceanogr. 40 (1995), https://doi.org/10.4319/lo.1995.40.3.0622.
[35] C. McAuliffe, Gas chromatographic determination of solutes by multiple phase equilibrium, Chem. Technol. (1971) 46–51.
[36] M.J. Pelczar, R.C. Bard, G.W. Burnett, H.J. Conn, R.D. Demoss, E.E. Euans, F. A. Weiss, M.W. Jennison, A.P. Meckee, A.J. Riker, in: Society of American Bacteriology, McGraw Hill (Eds.), Manual of Microbiological Methods, USA, New York, 1957.
[37] A.W. Bauer, D.M. Perry, W.M. Kirby, Single-disk antibiotic-sensitivity testing of staphylococci: an analysis of technique and results, A.M.A. Arch. Intern. Med. 104 (2) (1959) 208–216, https://doi.org/10.1001/archinte.1959.00270080034004.
[38] A. Bankevich, S. Nurk, D. Antipov, A.A. Gurevich, M. Dvorkin, A.S. Kulikov, V. M. Lesin, S.I. Nikolenko, S. Pham, A.D. Prjibelski, A.V. Pyshkin, A.V. Sirotkin, N. Vyahhi, G. Tesler, M.A. Alekseyev, P.A. Pevzner, SPAdes: A new genome assembly algorithm and its applications to single-cell sequencing, J. Comput. Biol. 19 (5) (2012) 455–477, https://doi.org/10.1089/cmb.2012.0021.
[39] D.H. Parks, M. Imelfort, C.T. Skennerton, P. Hugenholtz, G.W. Tyson, CheckM: assessing the quality of microbial genomes recovered from isolates, single cells, and metagenomes, Genome Res. 25 (7) (2015) 1043–1055, https://doi.org/10.1101/gr.186072.114.
[40] K. Lagesen, P. Hallin, E.A. Rødland, H.H. Staerfeldt, T. Rognes, D.W. Ussery, RNAmmer: consistent and rapid annotation of ribosomal RNA genes, Nucleic Acids Res. 35 (9) (2007) 3100–3108, https://doi.org/10.1093/nar/gkm160.
[41] S.H. Yoon, S.M. Ha, S. Kwon, J. Lim, Y. Kim, H. Seo, J. Chun, Introducing EzBioCloud: a taxonomically united database of 16S rRNA gene sequences and whole-genome assemblies, Int. J. Syst. Evol. Microbiol. 67 (5) (2017) 1613–1617, https://doi.org/10.1099/ijsem.0.001755.
[42] J.R. Grant, E. Enns, E. Marinier, A. Mandal, E.K. Herman, C.Y. Chen, M. Graham, G. Van Domselaar, P. Stothard, Proksee: in-depth characterization and visualization of bacterial genomes, Nucleic Acids Res. 51 (W1) (2023) W484–w492, https://doi.org/10.1093/nar/gkad326.
[43] S.F. Altschul, W. Gish, W. Miller, E.W. Myers, D.J. Lipman, Basic local alignment search tool, J. Mol. Biol. 215 (3) (1990) 403–410, https://doi.org/10.1016/s0022-2836(05)80360-2.
[44] A.M. Eren, Ö.C. Esen, C. Quince, J.H. Vineis, H.G. Morrison, M.L. Sogin, T. O. Delmont, Anvi'o: an advanced analysis and visualization platform for 'omics data, PeerJ 3 (2015) e1319, https://doi.org/10.7717/peerj.1319.
[45] A.M. Eren, E. Kiefl, A. Shaiber, I. Veseli, S.E. Miller, M.S. Schechter, I. Fink, J. N. Pan, M. Yousef, E.C. Fogarty, F. Trigodet, A.R. Watson, Ö.C. Esen, R.M. Moore, Q. Clayssen, M.D. Lee, V. Kivenson, E.D. Graham, B.D. Merrill, A. Karkman, D. Blankenberg, J.M. Eppley, A. Sjödin, J.J. Scott, X. Vázquez-Campos, L. J. McKay, E.A. McDaniel, S.L.R. Stevens, R.E. Anderson, J. Fuessel, A. Fernandez-Guerra, L. Maignien, T.O. Delmont, A.D. Willis, Community-led, integrated, reproducible multi-omics with anvi'o, Nat. Microbiol. 6 (1) (2021) 3–6, https://doi.org/10.1038/s41564-020-00834-3.
[46] D. Hyatt, G.L. Chen, P.F. Locascio, M.L. Land, F.W. Larimer, L.J. Hauser, Prodigal: prokaryotic gene recognition and translation initiation site identification, BMC Bioinform. 11 (2010) 119, https://doi.org/10.1186/1471-2105-11-119.
[47] S.R. Eddy, Accelerated profile HMM searches, PLoS Comput. Biol. 7 (10) (2011) e1002195, https://doi.org/10.1371/journal.pcbi.1002195.
[48] M.D. Lee, GToTree: a user-friendly workflow for phylogenomics, Bioinformatics 35 (20) (2019) 4162–4164, https://doi.org/10.1093/bioinformatics/btz188.
[49] R.C. Edgar, MUSCLE: multiple sequence alignment with high accuracy and high throughput, Nucleic Acids Res. 32 (5) (2004) 1792–1797, https://doi.org/10.1093/nar/gkh340.
[50] S. Kumar, G. Stecher, K. Tamura, MEGA7: molecular evolutionary genetics analysis version 7.0 for bigger datasets, Mol. Biol. Evol. 33 (7) (2016) 1870–1874, https://doi.org/10.1093/molbev/msw054.
[51] M. Kanehisa, S. Goto, Y. Sato, M. Furumichi, M. Tanabe, KEGG for integration and interpretation of large-scale molecular data sets, Nucleic Acids Res. 40 (D1) (2012) D109–D114, https://doi.org/10.1093/nar/gkr988.

[52] T. Aramaki, R. Blanc-Mathieu, H. Endo, K. Ohkubo, M. Kanehisa, S. Goto, H. Ogata, KofamKOALA: KEGG Ortholog assignment based on profile HMM and adaptive score threshold, Bioinformatics 36 (7) (2020) 2251–2252, https://doi.org/10.1093/bioinformatics/btz859.
[53] L. Pritchard, R.H. Glover, S. Humphris, J.G. Elphinstone, I.K. Toth, Genomics and taxonomy in diagnostics for food security: soft-rotting enterobacterial plant pathogens, Anal. Methods 8 (1) (2016) 12–24, https://doi.org/10.1039/C5AY02550H.
[54] A.J. Page, C.A. Cummins, M. Hunt, V.K. Wong, S. Reuter, M.T. Holden, M. Fookes, D. Falush, J.A. Keane, J. Parkhill, Roary: rapid large-scale prokaryote pan genome analysis, Bioinformatics 31 (22) (2015) 3691–3693, https://doi.org/10.1093/bioinformatics/btv421.
[55] T. Seemann, Prokka: rapid prokaryotic genome annotation, Bioinformatics 30 (14) (2014) 2068–2069, https://doi.org/10.1093/bioinformatics/btu153.
[56] R.K. Aziz, D. Bartels, A.A. Best, M. DeJongh, T. Disz, R.A. Edwards, K. Formsma, S. Gerdes, E.M. Glass, M. Kubal, F. Meyer, G.J. Olsen, R. Olson, A.L. Osterman, R. A. Overbeek, L.K. McNeil, D. Paarmann, T. Paczian, B. Parrello, G.D. Pusch, C. Reich, R. Stevens, O. Vassieva, V. Vonstein, A. Wilke, O. Zagnitko, The RAST server: rapid annotations using subsystems technology, BMC Genomics 9 (2008) 1–15, https://doi.org/10.1186/1471-2164-9-75.
[57] D. Arndt, A. Marcu, Y. Liang, D.S. Wishart, PHAST, PHASTER and PHASTEST: tools for finding prophage in bacterial genomes, Brief. Bioinform. 20 (4) (2019) 1560–1567, https://doi.org/10.1093/bib/bbx121.
[58] C. Bertelli, M.R. Laird, K.P. Williams, Simon Fraser University Research Computing Group, B.Y. Lau, G. Hoad, F.S. Brinkman, Islandviewer 4: expanded prediction of genomic islands for larger-scale datasets, Nucleic Acids Res. 45 (W1) (2017) W30–W35, https://doi.org/10.1093/nar/gkx343.
[59] J. Goris, K.T. Konstantinidis, J.A. Klappenbach, T. Coenye, P. Vandamme, J. M. Tiedje, DNA–DNA hybridization values and their relationship to whole-genome sequence similarities, IJSEM 57 (1) (2007) 81–91, https://doi.org/10.1099/ijs.0.64483-0.
[60] E.A. Ozer, J.P. Allen, A.R. Hauser, Characterization of the core and accessory genomes of *Pseudomonas aeruginosa* using bioinformatic tools spine and AGEnt, BMC Genomics 15 (737) (2014) 1–17, https://doi.org/10.1186/1471-2164-15-737.
[61] T.J. Collins, ImageJ for microscopy, Biotechniques 43 (S1) (2007) S25–S30, https://doi.org/10.2144/000112517.
[62] J. Fu, D. Wang, Z. Tang, Y. Xu, J. Xie, R. Chen, P. Wang, Q. Zhong, Y. Ning, M. Lei, H. Mai, H. Li, H. Liu, J. Wang, H. Cheng, NIR-responsive electrospun nanofiber dressing promotes diabetic-infected wound healing with programmed combined temperature-coordinated photothermal therapy, J. Nanobiotechnol. 22 (384) (2024), https://doi.org/10.1186/s12951-024-02621-2.
[63] P.S. Rimada, A.G. Abraham, Comparative study of different methodologies to determine the exopolysaccharide produced by kefir grains in milk and whey, Lait 83 (1) (2003) 79–87, https://doi.org/10.1051/lait:2002051.
[64] J.L. Donadio, S.B.R. do Prado, C.G. Soares, R.I. Tamarossi, R. Heidor, F. S. Moreno, J.P. Fabi, Ripe papaya pectins inhibit the proliferation of colon cancer spheroids and the formation of chemically induced aberrant crypts in rats colons, Carbohydr. Polym. 331 (2024) 121878, https://doi.org/10.1016/j.carbpol.2024.121878.
[65] L. de Freitas Pedrosa, D. Kouzounis, H. Schols, P. de Vos, J.P. Fabi, Assessing high-temperature and pressure extraction of bioactive water-soluble polysaccharides from passion fruit mesocarp, Carbohydr. Polym. 335 (2024) 122010, https://doi.org/10.1016/j.carbpol.2024.122010.
[66] K.S. Egorova, P.V. Toukach, Carbohydrate structure database (CSDB): Examples of usage, in: K.F. Aoki-Kinoshita (Ed.), A Practical Guide to Using Glycomics Databases, Springer Japan, Tokyo, 2017, pp. 75–113, https://doi.org/10.1007/978-4-431-56454-6_5.
[67] S. Sarkar, G. Cabrera-Barjas, R.N. Singh, J.P. Fabi, S.J.M. Breig, T. Jaime, R. K. Sani, A. Banerjee, Unveiling a novel exopolysaccharide produced by *Pseudomonas alcaligenes* Med1 isolated from a Chilean hot spring as biotechnological additive, Sci. Rep. 14 (2024) 25058, https://doi.org/10.1038/s41598-024-74830-6.
[68] R.J. Ruch, K.A. Crist, J.E. Klaunig, Effects of culture duration on hydrogen peroxide-induced hepatocyte toxicity, Toxicol. Appl. Pharmacol. 100 (3) (1989) 451–464, https://doi.org/10.1016/0041-008X(89)90293-7.
[69] K. Shimada, K. Fujikawa, K. Yahara, T. Nakamura, Antioxidative properties of xanthan on the autoxidation of soybean oil in cyclodextrin emulsion, J. Agric. Food Chem. 40 (6) (1992) 945–948, https://doi.org/10.1021/jf00018a005.
[70] I.F.F. Benzie, J.J. Strain, The ferric reducing ability of plasma (FRAP) as a measure of "antioxidant power": the FRAP assay, Anal. Biochem. 239 (1) (1996) 70–76, https://doi.org/10.1006/abio.1996.0292.
[71] J.J. Shi, J.G. Zhang, Y.H. Sun, J. Qu, L. Li, C. Prasad, Z.J. Wei, Physicochemical properties and antioxidant activities of polysaccharides sequentially extracted from peony seed dreg, Int. J. Biol. Macromol. 91 (2016) 23–30, https://doi.org/10.1016/j.ijbiomac.2016.05.082.
[72] D.G. Cooper, B.G. Goldenberg, Surface-active agents from two Bacillus species, Appl. Environ. Microbiol. 53 (2) (1987) 224–229, https://doi.org/10.1128/aem.53.2.224-229.1987.
[73] S. Kumari, S.H.K. Annamareddy, S. Abanti, P.K. Rath, Physicochemical properties and characterization of chitosan synthesized from fish scales, crab and shrimp shells, Int. J. Biol. Macromol. 104 (2017) 1697–1705, https://doi.org/10.1016/j.ijbiomac.2017.04.119.
[74] J.C. Wang, J.E. Kinsella, Functional properties of novel proteins: Alfalfa leaf protein, J. Food Sci. 41 (1976) 286–292, https://doi.org/10.1111/j.1365-2621.1976.tb00602.x.
[75] B. Prakash, B.M. Veeregowda, G. Krishnappa, Biofilms: a survival strategy of bacteria, Curr. Sci. 85 (9) (2003) 1299–1307. https://www.jstor.org/stable/24108133.
[76] X. Hu, S. Zhao, F. Li, X. Zhang, Y. Pan, J. Lu, Y. Li, M. Bao, The structure, characterization and immunomodulatory potential of exopolysaccharide produced by Planococcus rifietoensis AP-5 from deep-sea sediments of the Northwest Pacific, Int. J. Biol. Macromol. 245 (2023) 125452, https://doi.org/10.1016/j.ijbiomac.2023.125452.
[77] L. Gan, X. Li, H. Zhang, R. Zhang, H. Wang, Z. Xu, B. Peng, Y. Tian, Preparation, characterization and functional properties of a novel exopolysaccharide produced by the halophilic strain Halomonas saliphila LCB169T, Int. J. Biol. Macromol. 156 (2020) 372–380, https://doi.org/10.1016/j.ijbiomac.2020.04.062.
[78] S.L.R.K. Kanamarlapudi, S. Muddada, Characterization of exopolysaccharide produced by *Streptococcus thermophilus* CC30, Biomed. Res. Int. (2017), https://doi.org/10.1155/2017/4201809.
[79] P. Insulkar, S. Kerkar, S.S. Lele, Purification and structural-functional characterization of an exopolysaccharide from Bacillus licheniformis PASS26 with in-vitro antitumor and wound healing activities, Int. J. Biol. Macromol. 120 (2018) 1441–1450, https://doi.org/10.1016/j.ijbiomac.2018.09.147.
[80] C. Sabando, W. Ide, M. Rodríguez-Díaz, G. Cabrera-Barjas, J. Castaño, R. Bouza, N. Müller, C. Gutiérrez, L. Barral, J. Rojas, F. Martínez, S. Rodríguez-Llamazares, A novel hydrocolloid film based on pectin, starch and *Gunnera tinctoria* and *Ugni molinae* plant extracts for wound dressing applications, Curr. Top. Med. Chem. 20 (4) (2020) 280–292, https://doi.org/10.2174/1568026620666200124100631.
[81] I. Uhliariková, M. Matulová, P. Capek, Optimizing acid hydrolysis for monosaccharide compositional analysis of Nostoc cf. linckia acidic exopolysaccharide, Carbohydr. Res. 508 (2021) 108400, https://doi.org/10.1016/j.carres.2021.108400.
[82] M.A. Leal Leal, D. Tovar Rodríguez, M.A. de Pablo Hernandez, M.A. Bonilla Gómez, G. Leone, N. Tchegliakova Nikolaevna, J. Sánchez Nieves, A. Molina Jurado, J.T. San Martín Lobos, The potential of Deception Island, Antarctica, as a multifunctional Martian analogue of astrobiological interest, Int. J. Astrobiol. 24 (3) (2025), https://doi.org/10.1017/S1473550425000023.
[83] K.L. Smith, R.J. Baldwin, R.S. Kaufmann, A. Sturz, Ecosystem studies at Deception Island, Antarctica: an overview, Deep-Sea Res. II Top. Stud. Oceanogr. 50 (2003) 1595–1609, https://doi.org/10.1016/S0967-0645(03)00081-X.
[84] L. Somoza, J. Martínez-Frías, J.L. Smellie, J. Rey, A. Maestro, Evidence for hydrothermal venting and sediment volcanism discharged after recent short-lived volcanic eruptions at Deception Island, Bransfield Strait, Antarctica, Mar. Geol. 203 (2004) 119–140, https://doi.org/10.1016/S0025-3227(03)00285-8.
[85] P. Fermani, G. Mataloni, B. Van de Vijver, Soil microalgal communities on an antarctic active volcano (Deception Island, South Shetlands), Polar Biol. 30 (11) (2007) 1381–1393, https://doi.org/10.1007/s00300-007-0299-6.
[86] A.G. Bendia, C.N. Signori, D.C. Franco, R.T.D. Duarte, B.J.M. Bohannan, V. H. Pellizari, A mosaic of geothermal and marine features shapes microbial community structure on Deception Island volcano, Antarctica, Front. Microbiol. 9 (2018) 899, https://doi.org/10.3389/fmicb.2018.00899.
[87] M.J. Amenábar, P.A. Flores, B. Pugin, F.A. Boehmwald, J.M. Blamey, Archaeal diversity from hydrothermal systems of Deception Island, Antarctica, Polar Biol. 36 (2013) 373–380, https://doi.org/10.1007/s00300-012-1267-3.
[88] A. Santos, F. Burgos, J. Martinez-Urtaza, L. Barrientos, Metagenomic characterization of resistance genes in Deception Island and their association with mobile genetic elements, Microorganisms 10 (7) (2022) 1432, https://doi.org/10.3390/microorganisms10071432.
[89] M. Kim, H.S. Oh, S.C. Park, J. Chun, Towards a taxonomic coherence between average nucleotide identity and 16S rRNA gene sequence similarity for species demarcation of prokaryotes, Int. J. Syst. Evol. Microbiol. 64 (Pt_2) (2014) 346–351, https://doi.org/10.1099/ijs.0.059774-0.
[90] M. Richter, R. Rosselló-Móra, Shifting the genomic gold standard for the prokaryotic species definition, Proc. Natl. Acad. Sci. 106 (45) (2009) 19126–19131, https://doi.org/10.1073/pnas.0906412106.
[91] T. Dzeha, C.D. Nyiro, D. Kardasopoulos, D. Mburu, J. Mwafaida, M.J. Hall, J. G. Burgess, Uv resistance of bacteria from the Kenyan marine cyanobacterium *moorea producens*, Microbiologyopen 8 (4) (2018), https://doi.org/10.1002/mbo3.697.
[92] D.J. Crowley, I. Boubriak, B.R. Berquist, M. Clark, E. Richard, L. Sullivan, S. DasSarma, S. McCready, The uvrA, uvrB and uvrC genes are required for repair of ultraviolet light induced DNA photoproducts in *Halobacterium* sp. NRC-1, Saline Syst. 2 (1) (2006) 11, https://doi.org/10.1186/1746-1448-2-11.
[93] W. Jiang, Y. Hou, M. Inouye, CspA, the major cold-shock protein of Escherichia coli, is an RNA chaperone, J. Biol. Chem. 272 (1) (1997) 196–202, https://doi.org/10.1074/jbc.272.1.196.
[94] H. Schröder, T. Langer, F.U. Hartl, B. Bukau, DnaK, DnaJ and GrpE form a cellular chaperone machinery capable of repairing heat-induced protein damage, EMBO J. 12 (11) (1993) 4137–4144, https://doi.org/10.1002/j.1460-2075.1993.tb06097.x.
[95] R.D. Sleator, C. Hill, Bacterial osmoadaptation: the role of osmolytes in bacterial stress and virulence, FEMS Microbiol. Rev. 26 (1) (2002) 49–71, https://doi.org/10.1111/j.1574-6976.2002.tb00598.x.
[96] A. Kumar, A. Alam, M. Rani, N.Z. Ehtesham, S.E. Hasnain, Biofilms: survival and defense strategy for pathogens, Int. J. Med. Microbiol. 307 (8) (2017) 481–489, https://doi.org/10.1016/j.ijmm.2017.09.016.
[97] S. Naveed, C. Li, X. Lu, S. Chen, B. Yin, C. Zhang, Y. Ge, Microalgal extracellular polymeric substances and their interactions with metal (loid) s: a review, Crit. Rev. Environ. Sci. Technol. 49 (19) (2019) 1769–1802, https://doi.org/10.1080/10643389.2019.1583052.

[98] L. Hao, Y. Guo, J.M. Byrne, F. Zeitvogel, G. Schmid, P. Ingino, J. Li, T.R. Neu, E. D. Swanner, A. Kappler, M. Obst, Binding of heavy metal ions in aggregates of microbial cells, EPS and biogenic iron minerals measured in-situ using metal-and glycoconjugates-specific fluorophores, Geochim. Cosmochim. Acta 180 (2016) 66–96, https://doi.org/10.1016/j.gca.2016.02.016.
[99] B.V. Mohite, S.H. Koli, S.V. Patil, Heavy metal stress and its consequences on exopolysaccharide (EPS)-producing Pantoea agglomerans, Appl. Biochem. Biotechnol. 186 (1) (2018) 199–216, https://doi.org/10.1007/s12010-018-2727-1.
[100] M. Sajjad, K.S. Kim, Studies on the interactions of Ca2+ and Mg2+ with EPS and their role in determining the physicochemical characteristics of granular sludges in SBR system, Process Biochem. 50 (6) (2015) 966–972, https://doi.org/10.1016/j.procbio.2015.02.020.
[101] P. del Buey, M.E. Sanz-Montero, O. Braissant, O. Cabestrero, P.T. Visscher, The role of microbial extracellular polymeric substances on formation of sulfate minerals and fibrous Mg-clays, Chem. Geol. 581 (2021) 120403, https://doi.org/10.1016/j.chemgeo.2021.120403.
[102] J.N. Nkoh, J. Yan, Z. Hong, R. Xu, M.A. Kamran, J. Jun, J. Li, An electrokinetic perspective into the mechanism of divalent and trivalent cation sorption by extracellular polymeric substances of Pseudomonas fluorescens, Colloids Surf. B Biointerfaces 183 (2019) 110450, https://doi.org/10.1016/j.colsurfb.2019.110450.
[103] I. Bourven, E. Joussein, G. Guibaud, Characterisation of the mineral fraction in extracellular polymeric substances (EPS) from activated sludges extracted by eight different methods, Bioresour. Technol. 102 (14) (2011) 124–7130, https://doi.org/10.1016/j.biortech.2011.04.058.
[104] P. Bramhachari, G.P. Nagaraju, Extracellular polysaccharide production by bacteria as a mechanism of toxic heavy metal biosorption and biosequestration in the marine environment, in: Marine pollution and microbial remediation, 2017, pp. 67–85, https://doi.org/10.1007/978-981-10-1044-6_5.
[105] P. Carçabal, R.A. Jockusch, I. Hünig, L.C. Snoek, R.T. Kroemer, B.G. Davis, D. P. Gamblin, I. Compagnon, J. Oomens, J.P. Simons, Hydrogen bonding and cooperativity in isolated and hydrated sugars: mannose, galactose, glucose, and lactose, J. Am. Chem. Soc. 127 (32) (2005) 11414–11425, https://doi.org/10.1021/ja0518575.
[106] P. Gupta, P.A. Pruthi, V. Pruthi, Role of exopolysaccharides in biofilm formation, in: Introduction to Biofilm Engineering, ACS Publications, 2019, pp. 17–57, https://doi.org/10.1021/bk-2019-1323.ch002.
[107] W. Yuning, K. Weiwen, L. Wenjuan, D. Zirong, Y. Peiheng, T. Juan, W. Zibo, Y. Jinlong, Q.I. Jianping, Research progress of natural saccharides and their derivatives as drug delivery materials, Chin. J. Nat. Med. 23 (2024) 1–20, https://doi.org/10.1016/S1875-5364(24)60737-5.
[108] S. Datta, S. Bhattacharya, Multifarious facets of sugar-derived molecular gels: molecular features, mechanisms of self-assembly and emerging applications, Chem. Soc. Rev. 44 (15) (2015) 5596–5637, https://doi.org/10.1039/c5cs00093a.
[109] R.P. Singh, A.J. Bijo, R.S. Baghel, C.R. Reddy, B. Jha, Role of bacterial isolates in enhancing the bud induction in the industrially important red alga *Gracilaria dura*, FEMS Microbiol. Ecol. 76 (2) (2011) 381–392, https://doi.org/10.1111/j.1574-6941.2011.0157.x.
[110] A. Omoike, J. Chorover, Spectroscopic study of extracellular polymeric substances from Bacillus subtilis: aqueous chemistry and adsorption effects, Biomacromolecules 5 (4) (2004) 1219–1230, https://doi.org/10.1021/bm034461z.
[111] B.V. Mohite, S.H. Koli, J.D. Rajput, V.S. Patil, T. Agarwal, S.V. Patil, Production and characterization of multifacet exopolysaccharide from an agricultural isolate, *Bacillus subtilis*, Biotechnol. Appl. Biochem. 66 (6) (2019) 1010–1023, https://doi.org/10.1002/bab.1824.
[112] U. Lakra, V.L. Singh Munda, V.K. Nigam, S.R. Sharma, Optimisation, characterization, and biological evaluation of novel exopolysaccharide from Bacillus licheniformis (BITSL006), Nat. Prod. Res. 38 (21) (2023) 3783–3792, https://doi.org/10.1080/14786419.2023.2265041.
[113] J. Wang, S. Nie, Application of atomic force microscopy in microscopic analysis of polysaccharide, Trends Food Sci. Technol. 87 (2019) 35–46, https://doi.org/10.1016/j.tifs.2018.02.005.
[114] W. Lee, P.E. Marszalek, X. Zeng, W. Yang, Mechanics of Polysaccharides, Molecular Manipulation with Atomic Force Microscopy, 2012.
[115] B.B. Wang, D.C. Peng, Y.P. Hou, H.J. Li, L.Y. Pei, L.F. Yu, The important implications of particulate substrate in determining the physicochemical characteristics of extracellular polymeric substances (EPS) in activated sludge, Water Res. 58 (2014) 1–8, https://doi.org/10.1016/j.watres.2014.03.060.
[116] B.B. Wang, X.T. Liu, J.M. Chen, D.C. Peng, F. He, Composition and functional group characterization of extracellular polymeric substances (EPS) in activated sludge: the impacts of polymerization degree of proteinaceous substrates, Water Res. 129 (2018) 133–142, https://doi.org/10.1016/j.watres.2017.11.008.
[117] M.M. Caruso, D.A. Davis, Q. Shen, S.A. Odom, N.R. Sottos, S.R. White, J.S. Moore, Mechanically-induced chemical chages in polymeric materials, Chem. Rev. 109 (11) (2009) 5755–5798, https://doi.org/10.1021/cr9001353.
[118] J. Genzer, R.R. Bhat, Surface-bound soft matter gradients, Langmuir 24 (6) (2008) 2294–2317, https://doi.org/10.1021/la7033164.
[119] I. Luzinov, S. Minko, V.V. Tsukruk, Adaptive and responsive surfaces through controlled reorganization of interfacial polymer layers, Prog. Polym. Sci. 29 (7) (2004) 635–698, https://doi.org/10.1016/j.progpolymsci.2004.03.001.
[120] A. Spanò, P. Laganà, G. Visalli, T.L.C. Maugeri Gugliandolo, In vitro antibiofilm activity of an exopolysaccharide from the marine thermophilic *Bacillus licheniformis* T14, Curr. Microbiol. 72 (2016) 518–528, https://doi.org/10.1007/s00284-015-0981-9.
[121] K. Sharma, N. Sharma, S. Handa, S. Pathania, Purification and characterization of novel exopolysaccharides produced from *Lactobacillus paraplantarum* KM1 isolated from human milk and its cytotoxicity, J. Genet. Eng. Biotechnol. 18 (1) (2020) 56, https://doi.org/10.1186/s43141-020-00063-5.
[122] R.P. Singh, M.K. Shukla, A. Mishra, P. Kumari, C.R. Reddy, B. Jha, Isolation and characterization of exopolysaccharides from seaweed associated bacteria *Bacillus licheniformis*, Carbohydr. Polym. 84 (3) (2011) 1019–1026, https://doi.org/10.1016/j.carbpol.2010.12.061.
[123] A. Spanò, C. Gugliandolo, V. Lentini, T.L. Maugeri, G. Anzelmo, A. Poli, B. Nicolaus, A novel EPS-producing strain of Bacillus licheniformis isolated from a shallow vent off Panarea Island (Italy), Curr. Microbiol. 67 (1) (2013) 21–29, https://doi.org/10.1007/s00284-013-0327-4.
[124] N.M. Dogan, G.A. Doganli, G. Dogan, O. Bozkaya, Characterization of extracellular polysaccharides (EPS) produced by thermal *Bacillus* and determination of environmental conditions affecting exopolysaccharide production, Int. J. Environ. Res. 9 (3) (2015) 1107–1116, https://doi.org/10.22059/ijer.2015.998.
[125] M.M. Jayakody, K.G. Kaushani, M.P.G. Vanniarachchy, I. Wijesekara, Hydrocolloid and water soluble polymers used in the food industry and their functional properties: a review, Polym. Bull. 80 (2023) 3585–3610, https://doi.org/10.1007/s00289-022-04264-5.
[126] P. Edebrink, P.E. Jansson, G. Widmalm, T. Holme, M. Rahman, The structures of oligosaccharides isolated from the lipopolysaccharide of *Moraxella catarrhalis* serotype B, strain CCUG 3292, Carbohydr. Res. 295 (1996) 127–146, https://doi.org/10.1016/s0008-6215(96)90132-9.
[127] F.A. Ganaie, J.S. Saad, S.W. Lo, L. McGee, S.D. Bentley, A.J. van Tonder, P. Hawkins, J.D. Keenan, J.J. Calix, M.H. Nahm, Discovery and characterization of pneumococcal serogroup 36 capsule subtypes, serotypes 36A and 36B, J. Clin. Microbiol. 61 (4) (2023) e0002423, https://doi.org/10.1128/jcm.00024-23.
[128] F.L. Lin, E. Vinogradov, C. Deng, S. Zeller, B.A. Green, K.U. Jansen, V. Pavliak, Identification of the common antigenic determinant shared by Streptococcus pneumoniae serotypes 33A, 35A, and 20 capsular polysaccharides, Carbohydr. Res. 380 (2013) 101–107, https://doi.org/10.1016/j.carres.2013.08.001.
[129] B.M.S. Seco, F.F. Xu, A. Grafmüller, N. Kottari, C.L. Pereira, P.H. Seeberger, Sequential linkage of carbohydrate antigens to mimic capsular polysaccharides: toward semisynthetic glycoconjugate vaccine candidates against *Streptococcus pneumoniae* serotype 14, ACS Chem. Biol. 15 (9) (2020) 2395–2405, https://doi.org/10.1021/acschembio.0c00360.
[130] P. Li, Q. Liu, H. Luo, K. Liang, J. Yi, Y. Luo, Y. Hu, Y. Han, Q. Kong, O-serotype conversion in Salmonella typhimurium induces protective immune responses against invasive non-typhoidal Salmonella infections, Front. Immunol. 8 (2017) 1647, https://doi.org/10.3389/fimmu.2017.01647.
[131] M.A. Liu, A. Kidambi, P.R. Reeves, The low level of O antigen in Salmonella enterica Paratyphi A is due to inefficiency of the glycosyltransferase WbaV, FEMS Microbiol. Lett. 368 (3) (2021), https://doi.org/10.1093/femsle/fnab009.
[132] M. Watanabe, Y. Aoyagi, A. Ohta, D.E. Minnikin, Structures of phenolic glycolipids from *Mycobacterium Kansasii*, Eur. J. Biochem. 248 (1) (1997) 93–98, https://doi.org/10.1111/j.1432-1033.1997.00093.x.
[133] O.V. Bystrova, B. Lindner, H. Moll, N.A. Kocharova, Y.A. Knirel, U. Zähringer, G. B. Pier, Structure of the lipopolysaccharide of *Pseudomonas aeruginosa* O-12 with a randomly O-acetylated core region, Carbohydr. Res. 338 (18) (2003) 1895–1905, https://doi.org/10.1016/S0008-6215(03)00290-8.
[134] J.D. King, E.F. Mulrooney, E. Vinogradov, B. Kneidinger, K. Mead, J.S. Lam, lfnA from *Pseudomonas aeruginosa* O12 and wbuX from *Escherichia coli* O145 encode membrane-associated proteins and are required for expression of 2,6-dideoxy-2-acetamidino-L-galactose in lipopolysaccharide O antigen, J. Bacteriol. 190 (5) (2008) 1671–1679, https://doi.org/10.1128/JB.01708-07.
[135] B. Liu, A. Furevi, A.V. Perepelov, X. Guo, H. Cao, Q. Wang, P.R. Reeves, Y. A. Knirel, L. Wang, G. Widmalm, Structure and genetics of Escherichia coli O antigens, FEMS Microbiol. Rev. 44 (6) (2020) 655–683, https://doi.org/10.1093/femsre/fuz028.
[136] A.L. Lewis, P. Toukach, E. Bolton, X. Chen, M. Frank, T. Lütteke, Y. Knirel, I. Schoenhofen, A. Varki, E. Vinogradov, R.J. Woods, N. Zachara, J. Zhang, J. P. Kamerling, S. Neelamegham, SNFG discussion group, cataloging natural sialic acids and other nonulosonic acids (NulOs), and their representation using the symbol nomenclature for glycans, Glycobiology 33 (2) (2023) 99–103, https://doi.org/10.1093/glycob/cwac072.
[137] S. Neelamegham, K. Aoki-Kinoshita, E. Bolton, M. Frank, F. Lisacek, T. Lütteke, N. O'Boyle, N.H. Packer, P. Stanley, P. Toukach, A. Varki, R.J. Woods, SNFG discussion group, updates to the symbol nomenclature for glycans guidelines, Glycobiology 29 (9) (2019) 620–624, https://doi.org/10.1093/glycob/cwz045.
[138] S. Jenny Angel, G. Vidyadharani, S. Santhosh, R. Dhandapani, Optimization and characterisation of thermo stable exopolysaccharide produced from *Bacillus licheniformis* WSF-1 strain, J. Environ. Polym. Degrad. 26 (9) (2018) 3824–3833, https://doi.org/10.1007/s10924-018-1261-0.
[139] X. Lu, J. Chen, Z. Guo, Y. Zheng, M.C. Rea, H. Su, X. Zheng, B. Zheng, S. Miao, Using polysaccharides for the enhancement of functionality of foods: a review, Trends Food Sci. Technol. 86 (2019) 311–327, https://doi.org/10.1016/j.tifs.2019.02.024.
[140] B. Reshma Nambiar, P. Selvam Sellamuthu, A. Babu Perumal, E. Rotimi Sadiku, G. Phiri, J. Jayaramudu, Characterization of an exopolysaccharide produced by *lactobacillus plantarum* HM47 isolated from human breast milk, Process Biochem. 73 (2018) 15–22, https://doi.org/10.1016/j.procbio.2018.07.018.

[141] R.E. Lobo, M.I. Gómez, G. Font de Valdez, M.I. Torino, Physicochemical and antioxidant properties of a gastroprotective exopolysaccharide produced by Streptococcus thermophilus CRL1190, Food Hydrocoll. 96 (2019) 625–633, https://doi.org/10.1016/j.foodhyd.2019.05.036.
[142] A. Patel, J.B. Prajapati, Food and health applications of exopolysaccharides produced by lactic acid bacteria, Adv. Dairy Res. 1 (2013) 107, https://doi.org/10.4172/2329-888X.1000107.
[143] M.P. Narsing Rao, R.N. Singh, R.K. Sani, A. Banerjee, Genome-based approach to evaluate the metabolic potentials and exopolysaccharides production of *Bacillus paralicheniformis* CamBx3 isolated from a Chilean hot spring, Front. Microbiol. 15 (2024), https://doi.org/10.3389/fmicb.2024.1377965.
[144] O. Ates, Systems biology of microbial exopolysaccharides production, Front. Bioeng. Biotechnol. 3 (2015), https://doi.org/10.3389/fbioe.2015.00200.
[145] Y. Cui, T. Xu, X. Qu, T. Hu, X. Jiang, C. Zhao, New insights into various production characteristics of Streptococcus thermophilus strains, Int. J. Mol. Sci. 17 (10) (2016) 1701, https://doi.org/10.3390/ijms17101701.
[146] Z.Q. Xiong, L.H. Kong, P.F.H. Lai, Y.J. Xia, J.C. Liu, Q.Y. Li, L.Z. Ai, Genomic and phenotypic analyses of exopolysaccharide biosynthesis in *Streptococcus thermophilus* S-3, JDS 102 (6) (2019) 4925–4934, https://doi.org/10.3168/jds.2018-15572.
[147] R. Wu, Y. Qin, Q. Shen, P. Li, The complete genome sequence of *Bacillus velezensis* LPL061, an exopolysaccharide-producing bacterium, 3 Biotech. 10 (6) (2020) 243, https://doi.org/10.1007/s13205-020-02228-y.
[148] M.A. Khalil, F.I. Sonbol, L.A. Al-Madboly, T.A. Aboshady, A.S. Alqurashi, S.S. Ali, Exploring the therapeutic potentials of exopolysaccharides derived from lactic acid bacteria and bifidobacteria: antioxidant, antitumor, and periodontal regeneration, Front. Microbiol. 13 (2022) 803688, https://doi.org/10.3389/fmicb.2022.803688.
[149] S. Li, R. Huang, N.P. Shah, X. Tao, Y. Xiong, H. Wei, Antioxidant and antibacterial activities of exopolysaccharides from *Bifidobacterium bifidum* WBIN03 and *Lactobacillus plantarum* R315, JDS 97 (12) (2014) 7334–7343, https://doi.org/10.3168/jds.2014-7912.
[150] X. Zhao, G. Chen, F. Wang, H. Zhao, Y. Wei, L. Liu, H. Zhang, Extraction, characterization, antioxidant activity and rheological behavior of a polysaccharide produced by the extremely salt tolerant *Bacillus subtilis* LR-1, LWT 162 (2022) 113413, https://doi.org/10.1016/j.lwt.2022.113413.
[151] N.K. Alharbi, Z.F. Azeez, H.M. Alhussain, A.M.A. Shahlol, M.O.I. Albureikan, M. G. Elsehrawy, G.S. Aloraini, M. El-Nablaway, E.M. Khatrawi, A. Ghareeb, Tapping the biosynthetic potential of marine *Bacillus licheniformis* LHG166, a prolific sulphated exopolysaccharide producer: structural insights, bio-prospecting its antioxidant, antifungal, antibacterial and anti-biofilm potency as a novel anti-infective lead, Front. Microbiol. 15 (2024) 1385493, https://doi.org/10.3389/fmicb.2024.1385493.
[152] Y. Wang, Z. Ahmed, W. Feng, C. Li, S. Song, Physicochemical properties of exopolysaccharide produced by lactobacillus kefiranofaciens ZW3 isolated from Tibet kefir, Int. J. Biol. Macromol. 43 (3) (2008) 283–288, https://doi.org/10.1016/j.ijbiomac.2008.06.011.
[153] E.J. Gudiña, M.R. Couto, S.P. Silva, E. Coelho, M.A. Coimbra, J.A. Teixeira, L. R. Rodrigues, Sustainable exopolysaccharide production by *Rhizobium viscosum* CECT908 using corn steep liquor and sugarcane molasses as sole substrates, Polymers 15 (1) (2023) 20, https://doi.org/10.3390/polym15010020.
[154] S. Faria, C.L. de Oliveira Petkowicz, S.A. Lemos de Morais, M.G. Hernandez Terrones, M.M. de Resende, F.P. de França, V.L. Cardoso, Characterization of xanthan gum produced from sugar cane broth, Carbohydr. Polym. 86 (2) (2011) 469–476, https://doi.org/10.1016/j.carbpol.2011.04.063.
[155] L. Bai, D. Xu, Y.M. Zhou, Y.B. Zhang, H. Zhang, Y.B. Chen, Y.L. Cui, Antioxidant activities of natural polysaccharides and their derivatives for biomedical and medicinal applications, Antioxidants (Basel, Switzerland) 11 (12) (2022) 2491, https://doi.org/10.3390/antiox11122491.
[156] J. Wang, S. Hu, S. Nie, Q. Yu, M. Xie, Reviews on mechanisms of *in vitro* antioxidant activity of polysaccharides, Oxid. Med. Cell. Longev. (2016) 5692852, https://doi.org/10.1155/2016/5692852.
[157] X. Pang, H. Wang, C. Guan, Q. Chen, X. Cui, X. Zhang, Impact of molecular weight variations in *Dendrobium officinale* polysaccharides on antioxidant activity and anti-obesity in *Caenorhabditis elegans*, Foods 13 (7) (2024) 1040, https://doi.org/10.3390/foods13071040.
[158] W. Zhang, X. Liu, X. Sun, R. Han, N. Yu, J. Liang, A. Zhou, Comparison of the antioxidant activities and polysaccharide characterization of fresh and dry *Dendrobium officinale Kimura et Migo*, Molecules 27 (19) (2022) 6654, https://doi.org/10.3390/molecules27196654.
[159] J. Zhang, X. Xu, X. Liu, M. Chen, B. Bai, Y. Yang, T. Bo, S. Fan, The separation, purification, structure identification, and antioxidant activity of *Elaeagnus umbellata* polysaccharides, Molecules 28 (18) (2023) 6468, https://doi.org/10.3390/molecules28186468.
[160] J.D. Desai, I.M. Banat, Microbial production of surfactants and their commercial potential, Microbiol. Mol. Biol. Rev. 61 (1) (1997) 47–64, https://doi.org/10.1128/mmbr.61.1.47-64.1997.
[161] V. Venugopal, Marine Polysaccharides: Food Applications, CRC press, Boca Raton, FL, USA, 2016, https://doi.org/10.1201/b10516.
[162] V. Petravić-Tominac, V. Zechner-Krpan, K. Berković, P. Galović, Z. Herceg, S. Srečec, I. Špoljarić, Rheological properties, water-holding and oil-binding capacities of particulate β-glucans isolated from spent brewer's yeast by three different procedures, Food Technol. Biotechnol. 49 (2011) 56–64.